Microglial and peripheral immune priming is partially sexually dimorphic in adolescent mouse offspring exposed to maternal high-fat diet

Maude Bordeleau
CHU de Quebec-Universite Laval
Chloé Lacabanne
McGill University
Lourdes Fernández de Cossío
University of California San Diego
Nathalie Vernoux
CHU de Quebec-Universite Laval
Julie C. Savage
CHU de Quebec-Universite Laval
Fernando González-Ibáñez
CHU de Quebec-Universite Laval
Marie-Eve Tremblay (evetremblay@uvic.ca)
CHU de Quebec-Universite Laval https://orcid.org/0000-0003-2863-9626

Research

Keywords: Hippocampus, Immune priming, Maternal high-fat diet, Microglia, Sex difference

Posted Date: May 8th, 2020

DOI: https://doi.org/10.21203/rs.3.rs-25000/v1

Version of Record: A version of this preprint was published on September 5th, 2020. See the published version at https://doi.org/10.1186/s12974-020-01914-1.

Abstract

Background

Maternal nutrition is critical for proper fetal development. While increased nutrient intake is essential during pregnancy, an excessive consumption of certain nutrients, like fat, can lead to long-lasting detrimental consequences on the offspring. Animal work investigating the consequences of maternal high-fat diet (mHFD) revealed in the offspring a maternal immune activation (MIA) phenotype associated with increased inflammatory signals. This inflammation was proposed as one of the mechanisms causing neuronal circuit dysfunction, notably in the hippocampus, by altering the brain-resident macrophages –microglia. However, the understanding of mechanisms linking inflammation and microglial activities to pathological brain development remains limited. We hypothesized that mHFD-induced inflammation could prime microglia by altering their specific gene expression signature, population density and/or functions.

Methods

We used an integrative approach combining molecular techniques, confocal and scanning electron microscopy, to investigate the effects of mHFD *vs* control diet on inflammatory priming, as well as microglial density, distribution, morphology, and ultrastructure in mice. These analyses were performed on the mothers, and/or their adolescent offspring at postnatal day (P) 30.

Results

Our study revealed that mHFD results in MIA defined by increased circulating levels of interleukin (IL)-6 in the mothers. This phenotype was associated with an exacerbated inflammatory response to peripheral lipopolysaccharide in mHFD-exposed offspring of both sexes. Microglial morphology was also altered and there were increased microglial interactions with astrocytes in the hippocampus CA1 of mHFD-exposed male offspring, as well as decreased microglia-associated extracellular space pockets in the same region of mHFD-exposed offspring of the two sexes. A decreased mRNA expression of the inflammatory-regulating cytokine *Tgfb1* and microglial receptors *Tmem119*, *Trem2* and *Cx3cr1* was additionally measured in the hippocampus of mHFD-exposed offspring, especially in males.

Conclusions

Here, we described how dietary habits during pregnancy and nurturing, particularly the consumption of an enriched fat diet, can influence peripheral immune priming in the offspring. We also found that microglia are affected in terms of gene expression signature, morphology and interactions with the hippocampal parenchyma, in a partially sexually dimorphic manner, which may contribute to the adverse neurodevelopmental outcomes on the offspring.

Background

Maternal obesity and dietary overconsumption are risk factors for several health conditions in the offspring, from metabolic syndrome to neurodevelopmental disorders [1–3]. In fact, excess weight has been on the rise in both middle and high income countries, affecting over one third of the global population and about 38.9 million pregnant women worldwide [4]. This increase in the number of overweight or obese pregnant women has been linked to several elements of modern-day environment such as urbanization rate and increased caloric supply [4], which are often associated with increased fast food consumption [5]. This global issue stresses the importance of studying the impact of energy-dense, high-sugar and high-fat food diets during pregnancy [5].

High-fat diet (HFD) successfully models in animals the excessive intake of energy-dense, high-sugar and high-fat food [6]. Of these overconsumed nutrients, fat is of utmost importance for brain growth and development [7]. However, several independent studies using different animal models of maternal (m)HFD have shown a broad range of lasting behavioral alterations in the offspring related to neurodevelopmental disorders from increased anxiety-like behaviors [8–13] to cognitive [8, 14–18], social and motor deficits [9]. Although the mechanisms linking mHFD to the neurodevelopmental alterations remain unclear, several pathological processes such as decreased placental function, hormonal dysregulation, epigenetic alterations [2] and increased central as well as systemic inflammation [1] have been proposed.

In the past decade, epidemiological studies identified "maternal immune activation" (MIA), which refers to maternal systemic inflammation, as a risk factor for several neurodevelopmental disorders [19–22]. This has mostly been observed and researched in the context of infection, where a tight association between bacterial or viral (e.g. influenza) infections during pregnancy and a higher incidence of neurodevelopmental disorders, such as schizophrenia, was uncovered in the progeny [19, 20, 23]. It is now known that MIA is not limited to infection [19, 20, 23] and may occur after exposure to a large variety of maternal environmental risk factors common to modern-day life including stress [24, 25], smoking, alcohol consumption [26], air pollution [27, 28] and dietary imbalance or overconsumption such as HFD [1]. *Postmortem* studies revealed neuroimmune alterations in the brain of individuals with developmental disorders, as highlighted by the alteration of microglia –the brain-resident macrophages, in terms of morphology and gene expression signature [29–31], together with changes in the brain levels of cytokines –the molecules involved in signalling and modulation of the inflammatory state, among other important functions [19, 20, 23].

In animal models of mHFD, the inflammatory status in the offspring brain, notably in hippocampus, has been characterized by measuring changes of several inflammatory mediators during the lifespan. The mRNA expression of *Cd11b* and *Tlr4* – two genes involved in the innate immune response– were found to be increased in the hippocampus of male and female rat offspring as early as postnatal day (P)1, followed by *interleukin* (*Il*) *1β* at juvenile stages [8]. During adolescence, both male and female rat offspring exhibited greater levels of the cytokine *Il6*, as well as of the inflammatory regulators *nuclear factor κb* (*Nfκb*) and *mitogen-activated kinase protein* (*Mkp*) *1* in the hippocampus [32]. Adolescent male rat offspring also expressed increased levels of *Nfκb inhibitor* (*IκB*) in the hippocampus. Later in adult life, a few studies observed no change in cytokines [10] while others found greater expression of *Il1β* in the hippocampus of male rats [8], and lower expression of *IκB* and *Il1ra* in the hippocampus of female rats [13] exposed to mHFD. However, it remains unclear if this increased gene expression of inflammatory mediators is directly linked to a global inflammatory status or to altered microglial activities in the offspring brain. So far, the reported microglial changes induced by mHFD in the offspring brain comprise a higher density of ionized calcium-binding adapter 1 (IBA1)-positive ($^{+}$) cells in the hippocampus of adult male and female rats [8] suggesting changes in microglial function.

Studies performed in animal models and human *postmortem* samples have revealed that microglia modulate key neurodevelopmental processes –cell migration and maturation, followed by the formation of neuronal circuits and myelination– in a sexually dimorphic manner [33–35]. Microglia also contribute to neuronal circuit refinement during adolescence [36] and adulthood [29, 35, 37–39]. Paralleling the immune alterations described above, mHFD was shown to be associated with synaptic changes resulting in decreased synapses density and/or spines density and stability in rodent offspring across brain regions and stages of the lifespan [16, 25, 40–42] including the hippocampus of adolescent mice [16]. Microglial cell density, distribution, gene expression signature, physiological functions and/or response to immune challenges may be altered upon exposure to various environmental factors, thus impacting on their sculpting of the brain network [43, 44]. This phenomenon is referred to as immune priming [43, 44]. Studying microglial priming during sensitive periods like adolescence, in which the brain and especially the hippocampus experience important synaptic changes, may help to understand the pathological cascade underlying mHFD.

Using a mouse model, we explored the changes of microglia in the offspring exposed to mHFD *vs* control diet (CD). Specifically, we investigated microglia-related gene expression in whole hippocampus, as well as microglial density,

distribution, morphology and ultrastructure in the dorsal hippocampus CA1. We focused on this region considering its crucial importance for memory, learning [45, 46] and executive [47] functions that are affected with MIA [19–22] including with mHFD [8, 15, 16, 42]. The measurements were made at P30, which corresponds to early adolescence [48]. To characterize our model, we also assessed metabolic changes in the mothers and offspring, together with peripheral immune priming in the adolescent offspring, using a single systemic immune challenge with lipopolysaccharide (LPS) at P30. Male and female offspring were compared in all experiments to investigate possible sex differences.

Methods

Animal and tissue processing

All animal protocols were approved by McGill University's Facility Animal Care Committee under the guidelines of the Canadian Council on Animal Care. Mice were submitted to 12 hours dark/light cycles (8:00–20:00) with an *ad libitum* access to water and food. They were housed two to five per cage, except during pregnancy and nurturing, when the dams were housed single or alone with their litter.

Paired-housed C57BL/6N female mice aged 5–6 weeks were obtained from Charles River (St-Constant, QC, Canada) and habituated for one week prior to the protocol onset. They were then provided with either a HFD (diet rich in saturated and unsaturated fats; 60% kcal by lipids; Teklad TD.06414, ENVIGO, Indianapolis, IN, United States; Supplementary Fig. 1e) or CD (Teklad 2014, ENVIGO; Supplementary Fig. 1e) *ad libitum* starting 4 weeks prior to mating, throughout gestation and nurturing, until weaning of their litter (Fig. 1). During the diet protocol, food consumption and weight were recorded in the dams to identify potential metabolic changes. Blood samples were collected by submandibular puncture after 8 weeks on the diet to evaluate the inflammatory profile and assess circulating glucose levels. Dams were anesthetized with a rodent cocktail (0.3 mL/100 g) containing ketamine [100 mg/mL], xylazine [20 mg/mL] and aceprozamine [10 mg/mL], fresh-decapitated at the end of the protocol, after 9–10 weeks on the diet, and their fat deposits were dissected (Fig. 1).

Male and female offspring were compared to study mHFD effects in the two sexes. Animals presenting major anomalies (e.g. unopened or abnormal eye, dwarf or severe tooth malformation) were excluded. Only 1–2 offspring of each sex per litter were used for each experiment to prevent litter effects. At P21, the offspring were weaned and switched to CD. At P30, offspring were anesthetized with rodent cocktail and their blood, brain and fat tissues were collected. One cohort of offspring (n = 5–6 animal/sex/diet) was fresh-decapitated, their brain rapidly extracted, and the hippocampus dissected, flash-frozen on dry ice and stored at -80 °C until mRNA analysis by real-time quantitative polymerase chain reaction (rt-qPCR). Another cohort of offspring was anesthetised as described above, perfused with 15 mL of phosphate-buffered saline (PBS) followed by ~ 180 mL of 4% paraformaldehyde (PFA) in [50mM] phosphate-buffer (PB) for histological analysis (n = 5 animals/sex/diet). PFA-fixed brains were post-fixed in 4% PFA for 24 hours at 4^{o}C, then immersed in 30% glucose solution (in [50mM] PBS), pH = 7.4) at -4 °C for 48 hours and flash-frozen. Frozen brains were cut into 30 µm-coronal sections using a cryostat (CM3050S, Leica Biosystems, Wetzlar, Germany) and stored free-floating in cryoprotectant (30% ethylene glycol, 30% glycerol in [50mM] PBS, pH = 7.4) at -20 °C until use for histochemistry. The last cohort of animals was anesthetised as described above, flushed with 15 mL of PBS and perfused with 75 mL of 3.5% acrolein in [100mM] PB (pH = 7.4) and 150 mL of 4% PFA in [100mM] PB (pH = 7.4) for ultrastructural analysis (n = 4 animals/sex/diet). PFA/acrolein-fixed brains were post-fixed for 2 hours in 4% PFA at 4^{o}C, washed in PBS, cut into 50 µm-coronal sections with a vibratome (VT1200S, Leica Biosystems) and stored in cryoprotectant solution at -20 °C until use (Fig. 1).

Adolescent peripheral immune challenge

To evaluate peripheral immune priming, a subset of animals (n = 5–7 animals/sex/diet/treatment) received a single intraperitoneal injection at P30, of either 100 µg/kg lipopolysaccharide (LPS) from *Escherichia coli* O111:B4 (cat# 62325,

Millipore Sigma, Burlington, MA,United States) –a component of the gram-negative bacterial wall used to model an inflammatory response– or saline (SAL; 0.9% NaCl solution, cat# 01966010, Hospira, United States). Eight hours after the administration, animals were anesthetized with rodent cocktail (0.3 mL/100 g) and decapitated. Trunk blood was collected in heparinized tubes and centrifuged at 3600 rpm for 10 minutes. Plasma was collected and flash-frozen and stored at -80 °C until analysis by multiplex-ELISA (see section *Cytokines measurement by multiplex-ELISA*) (Fig. 1).

Physiological changes

To determine the phenotype induced by our diet model, a thorough characterization of the gestation and litter, as well as metabolic changes including weight, food intake, fat distribution and glucose levels was performed in the dams. The methods and results are presented as Supplementary material.

Cytokine measurement by multiplex-ELISA

To determine changes in the inflammatory profile of the dams, peripheral inflammation was assessed at the end of nurturing (after 8–9 weeks on the diet) (n = 5–6 dams/diet). Similarly, the peripheral inflammatory profile of the pubertal offspring (P30) was characterized in homeostatic (SAL-treated) *vs* immune (LPS-treated) contexts (n = 5–6 animals/sex/diet/treatment). Levels of the cytokines IL-1β, IL-6, IL-10, IL-17 and tumor necrosis factor (TNF)-α were measured in maternal and offspring plasma using Luminex Multiplex Assay (MILLIPLEX MAP kit Mouse Cytokine/Chemokine Magnetic Bead Panel, cat# MCYTOMAG-70K, Millipore Sigma). Prior to the experiment, the multiplex assay reader Luminex MAGPIX (ThermoFisher Scientific, Waltham, MA, United States) was calibrated (#cat MPXCALK25, Thermo Fisher Scientific) and its performance verified (#cat MPXPVERK25, Thermo Fisher Scientific) according to the manufacturers' guidelines. Plasma samples were diluted 1:2 by combining 30 µL of plasma with the provided drive fluid buffer. Immunoassays were performed following the manufacturer's instructions. Diluted plasma was incubated overnight (~ 16 hours) with primary antibodies at 4 °C, 1 hour with detection antibodies at room temperature and 30 minutes with Streptavidin-beads at room temperature. Samples were resuspended in 150 µL drive fluid and run through the Luminex MAGPIX to assess cytokines levels.

Real-time quantitative polymerase chain-reaction

At P30, the two hippocampi of each offspring (n = 5–6 animals/sex/diet) were homogenized in Trizol (cat#15596-026, Ambion, Austin, TX, United States) and RNA was extracted using the Trizol/chloroform method followed by an isopropanol precipitation. The RNA pellet was washed once in 75% ethanol, let dry, then eluted in Nuclease-free water (cat#AM9937, Ambion). Samples were dosed using the NanoDrop ND-1000 kit (ThermoFisher Scientific).

Genomic DNA was removed from 1 µg isolated RNA sample by enzymatic degradation (cat# G488, Applied Biological Materials Inc, Richmond, BC, Canada). Purified RNA was used to obtain complementary DNA (cDNA) by reverse transcriptase reaction with iScript 5X MasterMix (cat#1708890, BioRad Laboratories, Hercules, CA, United States) using a TI thermocycler (Biometra, Göttingen, Germany). Using diluted cDNA, rt-qPCR was performed with the SybrGreen technology and cycle threshold (Ct) was determined using a LightCycler 480 II (Roche, Basel, Switzerland). RT-qPCR measured the microglial function-related genes *Tmem119* (primer 5' - TTC TTC CGG CAG TAC GTG AT ; primer 3' - CGA GGA TGG GTA GTA GGC TG), *Aif1*(primer 5' – TCT GCC GTC CAA ACT TGA AG ; primer 3' – GCC ACT GGA CAC CTC TCT AA), *Trem2* (primer 5' – ACC CTC TAG ATG ACC AAG ATG C, primer 3' – TTG GGC ACC CTC GAA ACT C), *Cx3cr1* (primer 5' – CAA GCT CAC GAC TGC CTT CT ; primer 3' – TGT CCG GTT GTT CAT GGA GTT), *Tgfb1* (primer 5' – ACA TGT GGA ACT CTA CCA GAA A ; primer 3' – CTG CCG TAC AAC TCC AGT GA) as well as housekeeping gene *Rpl32* (primer 5'-TTG TTG CTC CCA TAA CCG ATG, primer 3'-TTA AGC GAA ACT GGC GGA AAC). Other than the cytokine *Tgfb1*, we attempted to assess mRNA levels of *Il1b* and *Il6*, however we failed to obtain robust amplification by rt-qPCR. Relative expression was calculated by determining the difference of Ct between the genes of interest and the housekeeping gene ($2^{-\Delta\Delta Ct}$), while arbitrarily considering CD-exposed male offspring as the reference group [49]. Results were presented in ratio fold and statistical analysis was assessed on ΔΔCt which are normally distributed.

Microglial density, distribution and morphology analysis

PFA-perfused brain sections were double-immunostained against IBA1 (labels all myeloid cells including microglia) and transmembrane protein 119 (TMEM119; microglia-specific [50]) to evaluate microglial density, distribution and morphology, as well as myeloid cell infiltration as previously described [51]. Three to four brain sections containing the dorsal hippocampus CA1 (Bregma: -1.31 to -1.91, stereotaxic atlas of Paxinos and Franklin 4th edition [52]) were selected for each offspring (n = 5 animals/sex/diet). Sections were washed, incubated 40 minutes in sodium citrate buffer to expose epitopes, washed again and treated with 0.1% $NaBH_4$ (cat#480886, MilliporeSigma) to quench autofluorescence. Afterwards, brain sections were incubated in blocking solution (0.5% gelatin, 5% donkey serum, 0.1% Triton X-100) for 1 hour at room temperature, washed and incubated overnight at 4 °C with a cocktail of primary antibodies in blocking solution: mouse anti-IBA1 (1:190; cat# MABN92, Millipore Sigma) and rabbit anti-TMEM119 (1:300; cat# ab209064, Abcam). The sections were washed and incubated with the secondary antibodies donkey anti-mouse Alexa555-conjugated (1:300 in PBS; cat#A31570, Invitrogen, ThermoFisher Scientific) and donkey anti-rabbit Alexa647-conjugated (1:300 in PBS; cat#A31573, Invitrogen, ThermoFisher Scientific) for 1.5 hour at room temperature. Sections were then mounted on slides and coverslipped in Fluoromount mounting medium (cat# 0100-01, SouthernBiotech, Birmingham, AB, United States).

For density and distribution analysis, all stained sections were imaged in a single plane at 20X using an Axio Imager M2 epifluorescence microscope equipped with an AxioCam MRm camera (Zeiss, Oberkochen, Germany). For morphology analysis, z-stacks (*stratum radiatum (st rad)*: 18–20 z-stacks/animal; *stratum lacunosum moleculare* (*st lac mol)*: 10–15 z-stacks/animal) were captured at 40X using a Quorum Wave FX spinning disc confocal microscope (Quorum Technologies, Guelph, ON, Canada) equipped with an ORCA-R2 camera (512 × 512 pixels; Hamamatsu Photonics, Hamamatsu, Japan). The z-stacks were merged into a single plane using Volocity software (Version 5.4, PerkinElmer, Waltham, MA, United States).

All analyses were performed blind to the experimental condition using ImageJ software (v1.51j8; National Institute of Health, Bethesda, MD, United States). Total count of $IBA1^+/TMEM119^+$ (microglia) and $IBA1^+/TMEM119^-$ (peripheral macrophages) cells was compiled for the dorsal hippocampus CA1, *st rad* and *st lac mol*, across 6–8 hippocampi per animal, using the analyze particles plugin [51, 53]. Afterwards, cellular distribution was assessed using the nearest neighbour distance (NDD) plugin. For microglial morphology analysis, the number of branches and junctions, as well as average and longest branch length were obtained (*st rad*: n = 20–25 microglia/animal, *st lac mol*: n = 15–20 microglia/animal, N = 5 animals/sex/diet) using a semi-automatic method adapted from [54]. For each microglial cell, soma and manual arbor were also traced using the freehand tool and polygon selection tool to obtain area values. Morphological index for each microglia was calculated by dividing the soma area by the manual arborization area to help identify microglial changes from their steady state [51, 53]. Manual arbor selection was further processed in a semi-automated manner to obtain unsharp mask of the cell, adjusted by the observer when needed, and area of the cell and shape descriptors (i.e. circularity, solidity and aspect ratio) values were measured. Circularity was calculated by: $4\pi\times(\text{Area}/\text{Perimeter}^2)$, for which a value of 1.0 represent a perfect circle and towards 0.0 an elongated shape. Solidity was calculated by dividing the cell area by the convex cell area meaning that a value close to 0.0 indicate a porous shape and close to 1.0 a convex shape. Finally, the aspect ratio was calculated by dividing the major axis of the cell by the minor axis of the cell, meaning a value of 1.0 similar ratio of minor and major axis and the higher the value the more elongated the cell is. The mask of the cell was skeletonized and analyzed using skeleton 2D/3D plugin. Skeleton analysis allowed us to determine number, average length, and maximal length of branches as well as number of junctions.

Microglial ultrastructure analysis

Two PFA/acrolein-perfused brain sections containing the dorsal hippocampus CA1 (Bregma − 1.67 mm; stereotaxic atlas of Paxinos and Franklin 4th edition [52]) were selected in each of four animals per group. Sections were washed in PBS, then quenched 10 minutes in 0.3% H_2O_2 in PBS and permeabilized 30 minutes in 0.1% $NaBH_4$ in PBS. Sections were first

incubated 1 hour at room temperature in blocking solution (10% fetal bovine serum, 3% bovine serum albumin, 0.01% Triton X-100 in [50mM] tris-buffered saline (TBS) before incubation with rabbit anti-IBA1 primary antibody (1:1000; cat#019-19741, FUJIFILM Wako Chemical, Osaka, Japan) in blocking solution overnight at 4 °C. The following day, antibody was washed out and the sections were incubated with biotinylated goat anti-rabbit secondary antibody (cat# 111-066-046, Jackson ImmunoResearch, West Grove, PA, United States) in TBS for 1.5 hour, followed by avidin-biotin complex solution (1:1:100 in TBS; cat# PK-6100,Vector Laboratories, Burlingame, CA, United States) for 1 hour. The staining was revealed in 0.05% diaminobenzidine (DAB; cat# D5905-50TAB, Millipore Sigma) with 0.015% H_2O_2 in TBS for 4.5 minutes at room temperature.

The immunostained sections were next post-fixed flat in osmium-thiocarbohydrazide-osmium for scanning electron microscopy (SEM). In particular, sections were incubated in 3% ferrocyanide (cat# PFC232.250, BioShop, Burlington, ON, Canada) diluted in water combined (1:1) with 4% aqueous osmium tetroxide (cat#19170, Electron Microscopy Sciences, Hatfield, PA, United States) for 1 hour, in 1% thiocarbohydrazide diluted in water (cat# 2231-57-4, Electron Microscopy Sciences) for 20 minutes, in 2% osmium tetroxide diluted in water, then dehydrated in ascending concentration of ethanol (2 × 35%, 50%, 70%, 80%, 90%, 3 × 100%) followed by propylene oxide (3x) for 5 minutes each. After post-fixation, tissues were embedded in Durcupan ACM resin (cat# 44611–44614, Millipore Sigma) for 24 hours and carefully placed between two ACLAR® embedding films (cat# 50425-25, Electron Microscopy Sciences) and the resin was let to polymerize at 55 °C for 72 hours. Regions of selection –dorsal hippocampus CA1– were excised from the embedded sections on ACLAR® sheets and re-embedded on top of a resin block for ultrathin sectioning (Ultracut UC7 ultramicrotome, Leica Biosystems). Ultrathin sections (~ 75 nm thickness) were collected and placed on a silicon nitride chip and glued on specimen mounts for SEM. Seven to 12 microglial cell bodies in each animal/layer of interest (*st rad* and *st lac mol*) were imaged at 5 nm of resolution using a Crossbeam 540 field emission SEM with a Gemini column (Zeiss).

Ultrastructural analysis was performed blind to the experimental conditions using ImageJ software (*st rad*: n = 32–41 microglia/sex/diet, *st lac mol*: n = 28–36 microglia/sex/diet, N = 4 animals/sex/diet). Microglial endoplasmic reticulum, Golgi apparatus, lysosomes, lipofuscin, mitochondria and endosomes were first analyzed quantitatively [55]. Dilation of the endoplasmic reticulum and/or Golgi apparatus was noted when the distance between the cisternal membranes was 50 nm or greater [56, 57]. Lysosomes were identified by their dense heterogeneous contents enclosed by a single membrane [58, 59]. Secondary lysosomes were differentiated from primary lysosomes by their contacts with fusion endosomes. Tertiary lysosomes were identified by their contacts with lipofuscin and often also with fusion endosomes [58, 60]. Lipofuscin granules, for their part, were identified by their oval- or round structure and finely granular composition with a unique fingerprint-like pattern [60]. Mitochondria were considered as elongated when their length was greater than 1 µm [55]. Microglial contacts with the cell bodies from other brain cells (i.e. astrocytes, neurons, oligodendrocytes) as well as blood vessels were quantified. For the neurons, contacted myelinated axons and synaptic elements –pre-synaptic axon terminal or post-synaptic dendritic spine– were further identified. Astrocytic cells were identified by their pale nuclei with a thin rim of heterochromatin and pale irregular cytoplasm, often containing intermediary filaments [61]. Neurons were distinguished by their pale nuclei and pale cytoplasm, often with an apical dendrite and innervation from axon terminals [61]. Pre-synaptic axon terminals were differentiated by their synaptic vesicles, while post-synaptic spines were in contact with a pre-synaptic axon terminal, often with a visible post-synaptic density at their junction [61]. Microglia were recognized by their dark irregular nuclei with a heterogenous chromatin pattern and a dark irregular cytoplasm, often containing short endoplasmic reticulum cisternae and lipidic inclusions (i.e. lipofuscin, lipid bodies or droplets, lysosomes) [61]. Similar to microglia, oligodendrocytes were identified by their dark nuclei with a heterogenous chromatin pattern and dark squarish or rectangular-shape cytoplasm, often containing short and wide endoplasmic reticulum cisternae organised in the vicinity of the nucleus and ribosomes, as well as a wider space between nuclear membranes than microglia [61]. In the vicinity of microglia, the occurrence of degradation activities (degenerating myelin, extracellular digestion) was also noted. Extracellular digestion, also named “exophagy”, was identified by extracellular space pockets containing degraded elements

or debris [62, 63]. In contrast, degenerating myelin was recognized by ballooning, swelling or distancing of myelin sheaths [61].

In addition, the density of dark cells and apoptotic cells was assessed (N = 4 animals/sex/diet). Then, dark cells were analyzed in a semi-quantitative manner (*st rad*: n = 0–6 dark cells/sex/diet, *st lac mol*: n = 13–19 dark cells/sex/diet, N = 4 animals/sex/diet). Dark cells were distinguished by their electron-dense nuclei showing a loss of the chromatin pattern and electron-dense cytoplasm presenting several signs of cellular stress (i.e. dilated endoplasmic reticulum and Golgi apparatus cisternae, elongated mitochondria) [64]. In the present study, we distinguished between two types of dark cells: microglia and perivascular cells. In addition to their dark features, dark microglia were recognised by their microglial characteristics [55, 64] and were located inside the brain parenchyma. Dark perivascular cells were identified by their localization enclosed in the perivascular space and possessed the dark features mentioned above. Apoptotic cells were also dark, and recognised with their pyknotic nucleus and accumulation of autophagic endosomes [65].

Sample size of dark cells in *st lac mol* (n = 59 individual dark cells total) was considered sufficient to attempt statistical data analysis. This assumption was based on the sample size calculated using G*Power software (v3.1.9.6) [66] to detect a large effect size of 0.4 that was estimated to 52 individuals cells.

Statistical analyses

Data are reported as means ± standard error of the mean (SEM). Sample size (n) refers to individual animals for metabolic parameters, immune priming, gene expression as well as microglial density and morphology analyses, while it refers to individual microglia or dark cells for ultrastructural analyses. Statistical analyses were conducted using Prism 8 (v.8.3, GraphPad Software, San Diego, CA, United States). Normality was verified using Shapiro-Wilk and assessed by QQ plot. For normally distributed dataset, Grubbs' test was used to identify outliers that were removed from the datasets prior to performing parametric statistic tests. To compare CD *vs* HFD in the dams, a Student t-test was used for non-repeated measures including glucose levels, weight and fat deposit measurements, while a 2-way analysis of variance (ANOVA) for repeated measures test was used for comparing weight and dietary follow up data across time. In the offspring, a 2-way ANOVA was used to compare CD *vs* mHFD, as well as male and female animals for metabolic parameters (i.e. weight and fat deposits), gene expression, as well as microglial density, distribution, morphology and ultrastructure. Significant ANOVA tests with a Sex*Diet interaction were followed by Bonferroni *post-hoc* test to identify significant differences between individual groups. For non-normally distributed dataset, a Mann-Whitney test was used to compare CD *vs* HFD in the dams for cytokines profile, gestation duration and litter size. For non-normally distributed offspring dataset, a mixed-effect model was used to compare CD *vs* mHFD, males *vs* females in terms of myeloid cells infiltration, as well as to compare SAL *vs* LPS groups after immune challenge to assess cytokines profile. Significant mixed-effect model was followed by a Bonferroni *post-hoc* test. Statistically significant differences were considered for p value < 0.05.

Results

High-fat diet induces long-term increase of peripheral IL-6 and fat deposits in dams and male offspring

Previously, rodent models of mHFD were shown to induce peripheral inflammation, notably by increasing the levels of cytokines in maternal blood circulation [14, 28, 67, 68]. To evaluate the maternal immune profile in our mouse model of mHFD, we measured plasma levels of pro- (IL-1β, IL-6, IL-17, TNF-α) and anti-inflammatory (IL-6, IL-10) cytokines in the dams at weaning of their litter by multiplex-ELISA. Plasma levels of IL-6 were significantly increased (p = 0.0079) in HFD-fed dams (17.74 ± 8.79 pg/mL) compared to CD-fed dams (3.636 ± 0.933 pg/mL) (Fig. 2d), while both diet groups had similar levels of IL-1 β, IL-10, IL-17 and TNF-α (Fig. 2a-b, e). Overall, these results suggest a MIA phenotype induced by mHFD in our model, confirmed by the increase of IL-6.

Other than peripheral inflammation, HFD has been associated with a variety of metabolic changes including increased body fat, obesity, diabetic-like phenotype (glucose and/or insulin intolerance) [69] and decreased fertility [70]. To characterize further our model, we assessed weight and food consumption, glucose levels, fat deposits, as well as gestation duration and litter size in the dams. These measurements revealed that mHFD does not induce obesity, although it is associated with an overconsumption of fats to the detriment of carbohydrates (Supplementary Fig. 1). HFD nevertheless resulted in an increase of retroperitoneal, subcutaneous and perigonadal fat deposition at the measured endpoint, without driving an overall increase of total body mass or an obese phenotype (Supplementary Fig. 2). Importantly, it did not lead to glycemia or fertility alterations, ruling out major metabolic alterations as often seen in diet-induced animal models of obesity (Supplementary Fig. 2).

Previous work on mHFD revealed that offspring are more prone to developing metabolic syndrome, which includes increase in fat deposits and body weight [2]. In our study, mHFD offspring had similar body weight compared to CD offspring at P30, but the mHFD males showed increased perigonadal fat deposits compared to CD males (Supplementary Fig. 3), which highlights a sexually dimorphic effect of mHFD on offspring fat deposition.

mHFD offspring have higher IL-6 plasma levels after LPS-induced immune challenge

To assess peripheral immune priming in the adolescent offspring, we measured circulating cytokines by multiplex ELISA at P30, eight hours after systemic injection of low dose LPS *vs* SAL. This time point corresponds to a period of inflammatory resolution after the immune challenge. In LPS-injected animals, plasma levels of IL-6 were significantly elevated ($F_{(1,37)}$ = 10.44, p = 0.0317) in mHFD *vs* CD offspring regardless of their sex (436.8 ± 107.0 pg/mL *vs* 197.9 ± 74.1 pg/mL) (Fig. 3d). Moreover, regardless of their maternal diet, LPS-treated female offspring had significantly ($F_{(1,37)}$ = 5.324, p = 0.0004) increased plasma levels of IL-6 compared to LPS-treated male offspring (504.1 ± 113.8 pg/mL *vs* 152.3 ± 44.0 pg/mL) (Fig. 3d). Levels of TNF-α and IL-10 were also significantly increased (TNF-α: $F_{(1,37)}$ = 16.43, p = 0.0002; IL-10: $F_{(1,21)}$ = 30.63, p < 0.0001) in LPS-treated offspring compared to SAL-treated offspring regardless of their sex or maternal diet (TNF-α: 15.23 ± 2.66 pg/mL *vs* 4.435 ± 0.745 pg/mL; IL-10: 82.54 ± 8.03 pg/mL *vs* 10.76 ± 7.40 pg/mL) (Fig. 3c, e-f). Finally, levels of IL-1β and IL-17 were similar between SAL-treated and LPS-treated offspring regardless of their sex and maternal diet (Fig. 3a-b, f). Together, these results indicate that systemic LPS administration induced IL-6, IL-10 and TNF-α release detected eight hours afterwards in CD and mHFD offspring, while IL-6 release was significantly exacerbated in mHFD offspring, indicating either a sustained inflammation or a stronger response to the immune challenge specific to this cytokine upon exposure to mHFD.

Male offspring have altered gene expression after mHFD whereas both male and female offspring exhibit altered microglial morphology

Other than a peripheral inflammatory response, immune priming has been associated with changes in gene expression and/or morphology of immune cells –including microglia in the brain [1, 28, 72]. To characterize microglia-related gene changes, we used rt-qPCR to study mRNA expression in whole hippocampus of mHFD *vs* CD offspring at P30 (Fig. 4a). We focused on *Tgfb1* –a cytokine that modulates inflammation and microglia survival [73]– as well as on receptors mainly expressed by microglia in the brain that are involved with the regulation of inflammation (i.e. *Aif1* [74]), microglial survival (i.e. *Tmem119* [50], *Trem2* [75]) or synaptic remodeling (i.e. *Cx3cr1* [76–78], *Trem2* [76, 79–81]). mHFD-exposed male offspring had significantly reduced expression of *Tgfb1* ($F_{(1,19)}$ = 10.05, CD male: p = 0.0045, CD female: p = 0.0018, mHFD female: p = 0.0008) compared to other offspring groups (detailed in Table 1; Fig. 4b). Expression of *Aif1* was however similar between groups (Fig. 4c). mHFD-exposed male offspring also had a significantly lower ratio fold of *Tmem119* ($F_{(1,19)}$ = 19.47, CD male: p < 0.0001, CD female: p < 0.0001, mHFD female: p < 0.0001), *Trem2* ($F_{(1,19)}$ = 20.88, CD male: p <

0.0001, CD female: $p < 0.0001$, mHFD female: $p < 0.0001$) and *Cx3cr1* ($F_{(1,19)} = 16.44$, CD male: $p = 0.0002$, CD female: $p < 0.0001$, mHFD female: $p < 0.0001$) compared to the other offspring groups (detailed in Table 1; Fig. 4d-f). Together, these results indicate that mHFD leads to altered expression, specifically in males, of inflammatory-regulating (*Tgfb1*) as well as microglial function-related (*Tmem119*, *Trem2* and *Cx3cr1*) genes.

Table 1

mHFD effect on hippocampal mRNA levels of P30 offspring. Transcripts level of *Tgf1b*, *Aif1*, *Tmem119*, *Trem2* and *Cx3cr1* were normalized by *Rpl32*, where CD male offspring represent the reference group. $2^{-\Delta\Delta Ct}$: ratio fold compared to expression of the reference group, ΔΔCt: difference of cycle threshold between ΔCt of the target gene and ΔCt of *Rpl32*, CD: control diet, mHFD: maternal high-fat diet.

Gene	Male		Female		*F*	*p*
	CD	mHFD	CD	mHFD		
Tgfb1	$2^{-\Delta\Delta Ct}$=1.000 ΔΔCt = 0.000 ± 0.218	$2^{-\Delta\Delta Ct}$=0.2764 ΔΔCt = 1.860 ± 0.262	$2^{-\Delta\Delta Ct}$=1.139 ΔΔCt=-0.190 ± 0.407	$2^{-\Delta\Delta Ct}$=1.282 ΔΔCt=-0.360 ± 0.335	Sex*Diet:10.05 Sex: 14.16 Diet: 6.965	Sex*Diet:**0.0050** Sex: **0.0013** Diet: **0.0162**
Aif1	$2^{-\Delta\Delta Ct}$=1.000 ΔΔCt = 0.000 ± 0.328	$2^{-\Delta\Delta Ct}$= 0.7169 ΔΔCt = 0.480 ± 0.340	$2^{-\Delta\Delta Ct}$=1.069 ΔΔCt=-0.100 ± 0.290	$2^{-\Delta\Delta Ct}$=1.196 ΔΔCt= -0.260 ± 0.299	Sex*Diet:1.035 Sex: 1.783 Diet:0.2588	Sex*Diet:0.3218 Sex:0.1976 Diet:0.6168
Tmem119	$2^{-\Delta\Delta Ct}$=1.000, ΔΔCt = 0.000 ± 0.313	$2^{-\Delta\Delta Ct}$=0.1346 ΔΔCt = 2.89 ± 0.269	$2^{-\Delta\Delta Ct}$=1.260, ΔΔCt=-0.330 ± 0.350	$2^{-\Delta\Delta Ct}$=1.101, ΔΔCt=-0.140 ± 0.265	Sex*Diet:19.47 Sex: 30.15 Diet: 25.34	Sex*Diet:**0.0003** Sex:**<0.0001** Diet:**<0.0001**
Trem2	$2^{-\Delta\Delta Ct}$=1.000, ΔΔCt = 0.000 ± 0.282	$2^{-\Delta\Delta Ct}$=0.1690 ΔΔCt = 2.570 ± 0.229	$2^{-\Delta\Delta Ct}$=0.9781, ΔΔCt = 0.030 ± 0.326	$2^{-\Delta\Delta Ct}$=0.9598, ΔΔCt = 0.060 ± 0.242	Sex*Diet:20.88 Sex: 19.90 Diet: 21.88	Sex*Diet:**0.0002** Sex: **0.0003** Diet: **0.0002**
Cx3cr1	$2^{-\Delta\Delta Ct}$=1.000, ΔΔCt = 0.000 ± 0.203	$2^{-\Delta\Delta Ct}$=0.1724 ΔΔCt = 2.520 ± 0.479	$2^{-\Delta\Delta Ct}$=1.147, ΔΔCt=-0.200 ± 0.315	$2^{-\Delta\Delta Ct}$=1.207 ΔΔCt=-0.270 ± 0.276	Sex*Diet:16.44 Sex: 21.92 Diet: 14.71	Sex*Diet:**0.0007** Sex: **0.0002** Diet: **0.0011**

After performing rt-qPCR, we characterized the density, distribution, morphology and ultrastructure of microglia in mHFD *vs* CD-exposed offspring at P30. We focused on the dorsal hippocampus CA1, particularly the *st rad* and *st lac mol* –two main layers where neuronal plasticity occurs during cognitive processes [82] and that are associated to behavioral deficits previously reported in mHFD animal models [8, 14–18]. In both layers (Fig. 5a-e, n-r), the density and distribution of microglia ($IBA1^+/TMEM119^+$) and infiltrated myeloid cells ($IBA1^+/TMEM119^-$) were similar between groups (Table 2; Fig. 5j, w). Of note, infiltrated myeloid cells were marginal, accounting for 0.207% of IBA1 + cells in the *st rad* and 0.240% in *st lac mol*. Regardless of their sex and maternal diet, adolescent offspring displayed similar values for microglial soma, arbor and cell area, as well as morphological index (soma area/manual arborization area) in both CA1 *st rad* and *st lac mol* (Table 3–4; Fig. 5f-i, s-v). In *st rad*, further analysis of 'skeletonized' microglia revealed no significant difference between offspring groups in terms of number of branches, junctions, as well as average and maximal branch length (Table 3). However, shape descriptor analysis of microglia identified a significant decrease in their circularity value ($F_{(1,16)} = 4.683$, $p = 0.0459$) in mHFD offspring compared to controls (0.0265 ± 0.0004 *vs* 0.0295 ± 0.0006), but solidity and aspect ratio remained unchanged (Table 3; Fig. 5k-m). In *st lac mol*, microglia of mHFD-exposed offspring had significantly shorter branch length

($F_{(1,16)}$ = 4.553, p = 0.0487) compared to CD-exposed offspring (3.276 ± 0.015 µm *vs* 3.442 ± 0.022 µm) (Table 4; Fig. 5z). In addition to their shorter branch length, microglia of mHFD-exposed offspring had a significantly increased solidity ($F_{(1,16)}$ = 5.616, p = 0.0307) compared to CD offspring (0.2845 ± 0.0030 *vs* 0.2603 ± 0.0023), regardless of the sex (Table 4; Fig. 5y), which could indicate a difference in microglial arborization distribution and/or organization with mHFD. In this layer, microglial branch number, maximal branch length, junction number, circularity and aspect ratio were also similar between groups. Together, these morphological changes align with a microglial priming hypothesis, in which mHFD alters microglial morphology.

Table 2

mHFD effects on microglial density, distribution, and peripheral myeloid cell infiltration in the dorsal hippocampus CA1 of P30 offspring. %Infiltration: Average percentage of $IBA1^{+}/TMEM119^{-}$ cells on total myeloid cells count, a.u.: arbitrary unit, CD: control diet, *St lac mol*: *stratum lacunosum moleculare*, mHFD: maternal high-fat diet, *St rad*: *stratum radiatum*.

Parameters		Mean ± standard error of the mean				*F*	*p*
		Male		**Female**			
		CD	**mHFD**	**CD**	**mHFD**		
St rad	Density (cells/mm²)	228.5 ± 12.1	233.8 ± 2.1	225.4 ± 10.1	214.9 ± 5.4	Sex*Diet: 0.8838 Sex: 1.725 Diet: 0.09162	Sex*Diet: 0.3611 Sex: 0.2075 Diet: 0.7660
	Spacing Index (a.u.)	0.452 ± 0.014	0.469 ± 0.006	0.456 ± 0.011	0.454 ± 0.013	Sex*Diet: 0.6857 Sex: 0.2303 Diet: 0.4325	Sex*Diet: 0.4198 Sex: 0.6378 Diet: 0.5201
	Cluster	0.261 ± 0.138	0.051 ± 0.031	0.182 ± 0.084	0.222 ± 0.091	Sex*Diet: 1.759 Sex: 0.2359 Diet: 0.8177	Sex*Diet: 0.2034 Sex: 0.6338 Diet: 0.3793
	%Infiltration	0.201 ± 0.131	0.150 ± 0.092	0.270 ± 0.143	0.000 ± 0.000	Sex*Diet: 1.031 Sex: 0.1433 Diet: 2.241	Sex*Diet: 0.3250 Sex: 0.7100 Diet: 0. 1539
St lac mol	Density (cells/mm²)	248.8 ± 14.5	272.7 ± 14.2	239.4 ± 11.8	259.6 ± 15.0	Sex*Diet: 0.01730 Sex: 0.6481 Diet: 2.507	Sex*Diet: 0.8970 Sex: 0.4326 Diet: 0.1329
	Spacing Index (a.u.)	0.473 ± 0.019	0.466 ± 0.004	0.442 ± 0.016	0.470 ± 0.022	Sex*Diet: 1.105 Sex: 0.6448 Diet: 0.4185	Sex*Diet: 0.3089 Sex: 0.4337 Diet: 0.5268
	Cluster	0.122 ± 0.062	0.179 ± 0.093	0.029 ± 0.029	0.147 ± 0.065	Sex*Diet: 0.2179 Sex: 0.9011 Diet: 1.739	Sex*Diet: 0.6469 Sex: 0.3566 Diet: 0.2058
	%Infiltration	0.073 ± 0.073	0.437 ± 0.151	0.233 ± 0.154	0.216 ± 0.091	Sex*Diet: 2.421 Sex: 0.06043 Diet: 2.006	Sex*Diet: 0.1393 Sex: 0.8089 Diet: 0.1758

Table 3

mHFD effects on microglial morphological parameters in the dorsal hippocampus CA1 stratum radiatum **of P30 offspring**.
#: number, %: percentage on total myeloid cells, a.u.: arbitrary unit, CD: control diet, mHFD: maternal high-fat diet.

Parameters	Mean ± standard error of the mean				*F*	*p*
	Male		Female			
	CD	mHFD	CD	mHFD		
Soma area (µm²)	46.59 ± 1.92	46.88 ± 2.54	44.42 ± 1.38	45.82 ± 1.84	Sex*Diet: 0.08109 Sex: 0.6758 Diet: 0.1842	Sex*Diet: 0.7795 Sex: 0.4231 Diet: 0.6735
Arbor area (µm²)	1352.68 ± 154.93	1355.63 ± 112.22	1374.23 ± 160.96	1377.16 ± 129.59	Sex*Diet: 4.378 × 10^{-9} Sex: 0.02340 Diet: 0.0004357	Sex*Diet: >0.9999 Sex: 0.8803 Diet:0.9836
Morphological index (a.u.)	0.036 ± 0.003	0.035 ± 0.001	0.034 ± 0.003	0.035 ± 0.004	Sex*Diet: 0.09893 Sex: 0.1851 Diet: 0.0001109	Sex*Diet: 0.7572 Sex: 0.6728 Diet: 0.9917
Cell area (µm²)	425.49 ± 86.24	430.71 ± 55.12	473.40 ± 79.36	435.13 ± 49.86	Sex*Diet: 0.09819 Sex: 0.1422 Diet: 0.05674	Sex*Diet: 0.7581 Sex: 0.7110 Diet: 0.8148
Circularity (a.u.)	0.029 ± 0.001	0.027 ± 0.001	0.030 ± 0.001	0.027 ± 0.001	Sex*Diet: 0.03614 Sex: 0.7875 Diet: 4.683	Sex*Diet: 0.8516 Sex: 0.3880 Diet: **0.0459**
Solidity (a.u.)	0.281 ± 0.020	0.290 ± 0.018	0.302 ± 0.012	0.285 ± 0.006	Sex*Diet: 0.7345 Sex: 0.2907 Diet: 0.07122	Sex*Diet: 0.4041 Sex: 0.5972 Diet: 0.7930
Aspect ratio (a.u.)	1.666 ± 0.055	1.648 ± 0.053	1.633 ± 0.065	1.663 ± 0.069	Sex*Diet: 0.1587 Sex: 0.02512 Diet: 0.008885	Sex*Diet: 0.6956 Sex: 0.8761 Diet: 0.9261
# Branches	101.92 ± 21.70	104.47 ± 13.79	113.11 ± 17.14	102.23 ± 12.52	Sex*Diet: 0.1622 Sex: 0.07200 Diet: 0.06261	Sex*Diet: 0.6925 Sex: 0.7919 Diet: 0.8056

Parameters	Mean ± standard error of the mean				*F*	*p*
	Male		Female			
	CD	mHFD	CD	mHFD		
Average branch length (µm)	3.318 ± 0.127	3.218 ± 0.075	3.172 ± 0.071	3.237 ± 0.041	Sex*Diet: 0.9630 Sex: 0.5690 Diet: 0.04635	Sex*Diet: 0.3410 Sex: 0.4616 Diet: 0.8323
Longest branch (µm)	13.29 ± 0.24	13.26 ± 0.49	12.77 ± 0.21	13.99 ± 0.21	Sex*Diet: 4.048 Sex: 0.1145 Diet: 3.750	Sex*Diet: 0.0614 Sex: 0.7395 Diet: 0.0707
# Junctions	52.38 ± 12.05	53.49 ± 7.28	58.43 ± 9.08	52.28 ± 6.78	Sex*Diet: 0.1616 Sex: 0.07164 Diet: 0.07779	Sex*Diet: 0.6930 Sex: 0.7924 Diet: 0.7839

Table 4

mHFD effects on microglial morphological parameters in the dorsal hippocampus CA1 stratum lacunosum moleculare **of P30 offspring**. #: number, %: percentage on total myeloid cells, a.u.: arbitrary unit, CD: control diet, mHFD: maternal high-fat diet.

Parameters	Mean ± standard error of the mean				*F*	*p*
	Male		Female			
	CD	mHFD	CD	mHFD		
Soma area (µm²)	40.18 ± 1.74	42.45 ± 2.06	40.14 ± 0.92	40.64 ± 1.57	Sex*Diet: 0.2961 Sex: 0.3230 Diet: 0.7283	Sex*Diet: 0.5938 Sex: 0.5777 Diet: 0.4060
Arbor area (µm²)	988.76 ± 125.44	908.98 ± 111.46	974.04 ± 118.48	973.34 ± 157.09	Sex*Diet: 0.09350 Sex: 0.03685 Diet: 0.09685	Sex*Diet: 0.7637 Sex: 0.8502 Diet: 0.7597
Morphological index (a.u.)	0.043 ± 0.004	0.049 ± 0.005	0.044 ± 0.006	0.047 ± 0.009	Sex*Diet: 0.04385 Sex: 7.575×10^{-5} Diet: 0.5447	Sex*Diet: 0.8368 Sex: 0.9932 Diet: 0.4712
Cell area (µm²)	272.57 ± 46.35	272.50 ± 36.57	269.99 ± 40.25	283.11 ± 43.67	Sex*Diet: 0.02479 Sex: 0.009177 Diet: 0.02427	Sex*Diet: 0.8769 Sex: 0.9249 Diet: 0.8782
Circularity (a.u.)	0.028 ± 0.003	0.033 ± 0.003	0.031 ± 0.003	0.032 ± 0.006	Sex*Diet: 0.2333 Sex: 0.1162 Diet: 0.6419	Sex*Diet: 0.6357 Sex: 0.7377 Diet: 0.4348
Solidity (a.u.)	0.258 ± 0.012	0.287 ± 0.008	0.263 ± 0.007	0.282 ± 0.013	Sex*Diet: 0.2641 Sex: 0.004823 Diet: 5.616	Sex*Diet: 0.6144 Sex: 0.9455 Diet: **0.0307 ***
Aspect ratio (a.u.)	1.803 ± 0.089	1.787 ± 0.058	1.793 ± 0.078	1.752 ± 0.094	Sex*Diet: 0.02490 Sex: 0.07486 Diet: 0.1260	Sex*Diet: 0.8766 Sex: 0.7879 Diet: 0.7273

Parameters	Mean ± standard error of the mean				*F*	*p*
	Male		Female			
	CD	mHFD	CD	mHFD		
# Branches	72.83 ± 12.86	73.24 ± 9.70	73.90 ± 11.91	77.18 ± 12.65	Sex*Diet: 0.01466 Sex: 0.04465 Diet: 0.02438	Sex*Diet: 0.9052 Sex: 0.8353 Diet: 0.8779
Average branch length (µm)	3.464 ± 0.077	3.262 ± 0.048	3.420 ± 0.120	3.291 ± 0.037	Sex*Diet: 0.2168 Sex: 0.008423 Diet: 4.553	Sex*Diet: 0.6477 Sex: 0.9280 Diet: **0.0487**
Longest branch (µm)	13.61 ± 0.46	12.51 ± 0.55	12.96 ± 0.57	12.98 ± 0.61	Sex*Diet: 1.024 Sex: 0.02989 Diet: 0.9634	Sex*Diet: 0.3265 Sex: 0.8649 Diet: 0.3409
# Junctions	36.88 ± 6.99	37.01 ± 5.19	37.61 ± 6.37	39.29 ± 6.71	Sex*Diet: 0.01468 Sex: 0.05614 Diet: 0.02034	Sex*Diet: 0.9051 Sex: 0.8157 Diet: 0.8884

Microglia from mHFD male offspring show increased interactions with astrocytes whereas both male and female offspring have decreased extracellular space pockets

To provide insights into microglial functions, we further performed SEM analysis to reveal, at nanoscale resolution, possible changes in their organelles and intercellular relationships in the dorsal hippocampus CA1 of mHFD- *vs* CD-exposed offspring, upon sacrifice at P30. We determined the number of microglial organelles involved in phagolysosomal activity (primary, secondary and tertiary lysosomes, lipofuscin, endosomes with or without content) and alterations to organelles that serve as markers of cellular stress (dilated cisternae of endoplasmic reticulum and Golgi apparatus, elongated and total mitochondria). We also evaluated microglial interactions with their microenvironment, particularly direct contacts with astrocytic cell bodies, neuronal cell bodies, axon terminals, dendritic spines, oligodendrocytic cell bodies, myelinated axons, and blood vessels, as well as associations with extracellular space pockets containing degraded elements or debris indicative of extracellular digestion or “exophagy” [62, 63].

In the *st rad*, no significant difference in microglial organelles was observed between offspring groups, but there was a trend for a main diet effect regarding the total number of mitochondria per microglial cell body ($F_{(1,146)} = 3.870$, $p = 0.0511$) (Table 5). In terms of microglial interactions with their microenvironment, we detected a Sex*Diet interaction for the number of microglial contacts with astrocytes ($F_{(1,146)} = 0.0446$). *Post-hoc* analysis revealed that microglial cell bodies from mHFD-exposed male offspring made more cell-cell contacts with astrocytic cell bodies compared to CD male offspring ($p = 0.0182$, 0.225 ± 0.067 contacts *vs* 0.054 ± 0.038 contacts) (Table 5; Fig. 6a-e). Microglial interactions with synaptic elements, myelinated axons, neurons as well as oligodendrocytes remained unchanged (Table 5). We also identified a Sex*Diet

interaction for the prevalence of microglia-associated extracellular digestion ($F_{(1,146)}$ = 0.0433), however, *post-hoc* analysis revealed no significant different between offspring groups (Table 5).

Table 5

mHFD effects on microglial ultrastructure in the dorsal hippocampus CA1 stratum radiatum **of P30 offspring**. #: number, 1ary: primary, 2ary: secondary, 3ary: tertiary, Astro: astrocyte, CD: control diet, Dil ER/golgi: dilated endoplasmic reticulum and Golgi apparatus cisterna, Elong: elongated mitochondria, mHFD: maternal high-fat diet, Mito: mitochondria, N/A: not applicable, Oligo: oligodendrocyte.

Parameters			Mean ± standard error of the mean				*F*	*p*
			Male		**Female**			
			CD	**mHFD**	**CD**	**mHFD**		
Organelles	# Lysosomes	1ary	1.405 ± 0.461	1.150 ± 0.317	0.878 ± 0.213	1.438 ± 0.258	Sex*Diet: 1.552 Sex: 0.1344 Diet: 0.2160	Sex*Diet: 0.2149 Sex: 0.7144 Diet: 0.6428
		2ary	0.108 ± 0.052	0.200 ± 0.096	0.146 ± 0.075	0.188 ± 0.083	Sex*Diet: 0.1028 Sex: 0.02644 Diet: 0.7068	Sex*Diet: 0.7490 Sex: 0.8711 Diet: 0.4019
		3ary	0.027 ± 0.027	0.025 ± 0.025	0.000 ± 0.000	0.031 ± 0.031	Sex*Diet: 0.5148 Sex: 0.2007 Diet: 0.3970	Sex*Diet: 0.4742 Sex: 0.6548 Diet: 0.5296
	# Lipofuscin		0.135 ± 0.079	0.100 ± 0.048	0.073 ± 0.041	0.063 ± 0.043	Sex*Diet: 0.04895 Sex: 0.8091 Diet: 0.1716	Sex*Diet: 0.8252 Sex: 0.3699 Diet: 0.6793
	# Endosome	Empty	0.108 ± 0.052	0.200 ± 0.089	0.098 ± 0.058	0.063 ± 0.043	Sex*Diet: 0.9319 Sex: 1.267 Diet: 0.1867	Sex*Diet: 0.3360 Sex: 0.2621 Diet: 0.6663
		Content	0.432 ± 0.120	0.250 ± 0.128	0.268 ± 0.086	0.188 ± 0.070	Sex*Diet: 0.2278 Sex: 1.132 Diet: 1.528	Sex*Diet: 0.6339 Sex: 0.2890 Diet: 0.2185
	# Dil ER/golgi		5.892 ± 0.945	6.000 ± 1.046	6.171 ± 1.069	5.188 ± 0.723	Sex*Diet: Sex:	Sex*Diet: 0.5814

							Diet:	Sex: 0.7874 Diet: 0.6584
	# Mito	Elong.	0.459 ± 0.148	0.450 ± 0.138	0.293 ± 0.094	0.375 ± 0.087	Sex*Diet: 0.1409 Sex: 0.9777 Diet: 0.08878	Sex*Diet: 0.7080 Sex: 0.3244 Diet: 0.7662
		Total	2.270 ± 0.365	3.075 ± 0.486	2.195 ± 0.309	2.906 ± 0.322	Sex*Diet: 0.01475 Sex: 0.1002 Diet: 3.870	Sex*Diet: 0.9035 Sex: 0.7521 Diet: 0.0511
Interactions with microenvironment	# Synaptic terminal	Pre	6.243 ± 0.504	9.075 ± 0.958	7.683 ± 0.808	7.688 ± 0.647	Sex*Diet: 3.521 Sex: 0.008597 Diet: 3.111	Sex*Diet: 0.0701 Sex: 0.9732 Diet: 0.0692
		Post	3.081 ± 0.286	4.150 ± 0.438	3.707 ± 0.457	3.875 ± 0.559	Sex*Diet: 1.028 Sex: 0.1562 Diet: 1.936	Sex*Diet: 0.3123 Sex: 0.6933 Diet: 0.1663
	# Myelinated axon		0.135 ± 0.069	0.200 ± 0.089	0.073 ± .054	0.031 ± 0.031	Sex*Diet: 0.6218 Sex: 2.949 Diet: 0.02917	Sex*Diet: 0.4280 Sex: 0.0880 Diet: 0.8646
	# Degenerating myelin		0.216 ± 0.079	0.150 ± 0.067	0.098 ± 0.047	0.042 ± 0.042	Sex*Diet: 0.006245 Sex: 3.020 Diet:0.8740	Sex*Diet: 0.9371 Sex: 0.0845 Diet: 0.3515
	# Contacts with brain cells	Astro	0.054 ± 0.038	0.225 ± 0.067	0.049 ± 0.034	0.031 ± 0.031	Sex*Diet: 4.104 Sex: 4.576 Diet: 2.719	Sex*Diet: **0.0446** Sex: **0.0341** Diet: 0.1013
		Neuron	0.000	0.125	0.122	0.094	Sex*Diet:	Sex*Diet:

		± 0.000	± 0.053	± 0.052	± 0.052	2.771 Sex: 0.9714 Diet: 1.106	0.0981 Sex: 0.3260 Diet: 0.2946
	Oligo	0.000 ± 0.000	0.000 ± 0.000	0.000 ± 0.000	0.000 ± 0.000	N/A	N/A
	Blood vessel	0.189 ± 0.065	0.075 ± 0.042	0.073 ± 0.041	0.031 ± 0.031	Sex*Diet: 0.5805 Sex: 2.837 Diet: 2.709	Sex*Diet: 0.4473 Sex: 0.0942 Diet: 0.1019
# Extracellular space		0.216 ± 0.079	0.650 ± 0.146	0.537 ± 0.168	0.500 ± 0.168	Sex*Diet: 2.596 Sex: 0.3406 Diet: 1.851	Sex*Diet: 0.1093 Sex: 0.5604 Diet: 0.1757
# Extracellular digestion		0.135 ± 0.057	0.275 ± 0.101	0.366 ± 0.120	0.125 ± 0.059	Sex*Diet: 4.154 Sex: 0.1867 Diet: 0.2923	Sex*Diet: **0.0433** Sex: 0.6663 Diet: 0.5896

In *st lac mol*, microglial organelle content and ultrastructure were unaffected by offspring groups (Table 6), but their interactions with the microenvironment differed. Similar to microglia in the *st rad*, microglial cell bodies in *st lac mol* of mHFD-exposed male offspring had increased interactions with astrocytic cell bodies ($F_{(1,128)} = 4.604$, $p = 0.0446$) compared to CD male offspring (0.028 ± 0.028 contacts *vs* 0.214 ± 0.094 contacts) (Table 6; Fig. 6a-e, h-k, q). Of note, a significant main sex effect was also detected for microglial interactions with neurons ($F_{(1,128)} = 6.062$, $p = 0.0151$), where microglial cell bodies from male offspring compared to female offspring made more cell-cell contacts with neuronal cell bodies, regardless of maternal diet (0.081 ± 0.026 contacts *vs* 0.000 ± 0.000 contacts) (Table 6; Fig. 6h-k, r). Microglial interactions with synaptic elements, oligodendrocytes and myelinated axons were also unchanged across sex and diet groups (Table 6). Lastly, mHFD-exposed offspring had a significant decrease ($F_{(1,128)} = 7.666$, $p = 0.0065$) in microglia-associated extracellular space pockets compared to CD offspring (0.1374 ± 0.0768 contacts *vs* 0.5349 ± 0.0206 contacts) (Table 6; Fig. 6l-o, s) in the two sexes.

Table 6

mHFD effects on microglial ultrastructure in the dorsal hippocampus CA1 stratum lacunosum moleculare of P30 offspring. #: number, 1ary: primary, 2ary: secondary, 3ary: tertiary, Astro: astrocyte, CD: control diet, Dil ER/golgi: dilated endoplasmic reticulum and Golgi apparatus cisterna, Elong: elongated mitochondria, mHFD: maternal high-fat diet, Mito: mitochondria, N/A: not applicable, Oligodendrocyte.

Parameters			Mean ± standard error of the mean				*F*	*p*
			Male		Female			
			CD	mHFD	CD	mHFD		
Organelles	# Lysosomes	1ary	1.556 ±0.419	1.357 ±0.258	1.229 ±0.239	1.182 ±0.202	Sex*Diet: 0.06292 Sex: 0.6902 Diet: 0.1644	Sex*Diet: 0.8023 Sex: 0.4076 Diet: 0.6858
		2ary	0.361 ±0.090	0.250 ±0.098	0.229 ±0.092	0.212 ±0.104	Sex*Diet: 0.2389 Sex: 0.7742 Diet: 0.4337	Sex*Diet: 0.6259 Sex: 0.3806 Diet: 0.5113
		3ary	0.028 ±0.028	0.000 ±0.000	0.000 ±0.000	0.030 ±0.030	Sex*Diet: 1.817 Sex: 0.003435 Diet:0.003435	Sex*Diet: 0.1800 Sex: 0.9534 Diet: 0.9534
	# Lipofuscin		0.111 ±0.053	0.107 ±0.060	0.029 ±0.029	0.061 ±0.042	Sex*Diet: 0.1493 Sex: 1.918 Diet: 0.09070	Sex*Diet: 0.6999 Sex: 0.1684 Diet: 0.7638
	# Endosome	Empty	0.194 ±0.078	0.107 ±0.079	0.229 ±0.101	0.091 ±0.051	Sex*Diet: 0.09748 Sex: 0.01231 Diet: 1.945	Sex*Diet: 0.7554 Sex: 0.9118 Diet: 0.1655
		Content	0.361 ±0.144	0.214 ±0.079	0.171 ±0.077	0.152 ±0.063	Sex*Diet: 0.3989 Sex: 1.579 Diet: 0.6886	Sex*Diet: 0.5288 Sex: 0.2113 Diet: 0.4082
	# Dil ER/golgi		5.611 ±0.788	7.643 ±1.413	5.800 ±0.805	7.512 ±1.168	Sex*Diet: 0.1075	Sex*Diet: 0.7436

							Sex: 0.02125 Diet: 2.659	Sex: 0.8843 Diet: 0.1054
	# Mito	Elong	0.472 ±0.180	0.500 ±0.159	0.257 ±0.118	0.485 ±0.235	Sex*Diet: 0.3099 Sex: 0.4110 Diet:0.5061	Sex*Diet: 0.5787 Sex: 0.5226 Diet: 0.4781
		Total	3.111 ±0.534	2.071 ±0.430	2.400 ±0.341	2.970 ±0.543	Sex*Diet: 2.856 Sex: 0.03862 Diet: 0.2435	Sex*Diet: 0.0935 Sex: 0.8445 Diet: 0.6225
Interactions with microenvironment	# Synaptic terminal	Pre	6.250 ±0.745	5.821 ±0.587	5.171 ±0.527	5.125 ±0.442	Sex*Diet: 0.1168 Sex: 2.138 Diet: 0.1406	Sex*Diet: 0.7331 Sex: 0.1462 Diet: 0.7083
		Post	3.306 ±0.378	3.036 ±0.369	3.629 ±0.482	3.030 ±0.300	Sex*Diet: 0.1726 Sex: 0.1614 Diet: 1.206	Sex*Diet: 0.6785 Sex: 0.6885 Diet: 0.2742
	# Myelinated axon		0.417 ±0.108	0.536 ±0.167	0.486 ±0.161	0.545 ±0.151	Sex*Diet: 0.04059 Sex: 0.07164 Diet: 0.3689	Sex*Diet: 0.8406 Sex: 0.7894 Diet: 0.5447
	# Degenerating myelin		0.083 ±0.047	0.179 ±0.090	0.200 ±0.069	0.121 ±0.058	Sex*Diet: 1.763 Sex: 0.2047 Diet: 0.01575	Sex*Diet: 0.1867 Sex: 0.6517 Diet: 0.9003
	# Contacts with brain cells	Astro	0.028 ±0.028	0.214 ±0.094	0.114 ±0.055	0.061 ±0.042	Sex*Diet: 4.604 Sex: 0.3601 Diet: 1.408	Sex*Diet: **0.0338** Sex: 0.5495 Diet: 0.2376
		Neuron	0.056	0.107	0.000	0.000	Sex*Diet:	Sex*Diet:

		±0.039	±0.060	±0.000	±0.000	0.6095 Sex: 6.062 Diet: 0.6095	0.4364 Sex: **0.0151** Diet: 0.4364
	Oligo	0.000 ±0.000	0.036 ±0.036	0.000 ±0.000	0.000 ±0.000	Sex*Diet: 1.384 Sex: 1.384 Diet: 1.384	Sex*Diet: 0.2417 Sex: 0.2417 Diet: 0.2417
	Blood vessel	0.056 ±0.039	0.143 ±0.067	0.114 ±0.055	0.152 ±0.063	Sex*Diet: 0.2002 Sex: 0.3625 Diet: 1.238	Sex*Diet: 0.6553 Sex: 0.5482 Diet: 0.2679
# Extracellular space		0.556 ±0.176	0.214 ±0.094	0.514 ±0.180	0.061 ±0.042	Sex*Diet: 0.1533 Sex: 0.4611 Diet: 7.666	Sex*Diet: 0.6961 Sex: 0.4984 Diet: **0.0065**
# Extracellular digestion		0.528 ±0.216	0.321 ±0.219	0.200 ±0.090	0.364 ±0.105	Sex*Diet: 1.231 Sex: 0.7334 Diet: 0.01641	Sex*Diet: 0.2693 Sex: 0.3934 Diet:0.8983

Dark microglia and perivascular cells display increased number of dilated endoplasmic reticulum and Golgi apparatus cisterna in mHFD offspring

Previously, our laboratory identified a microglial subset, the “dark microglia”, which are characterized by a distinct ultrastructural signature compared with typical microglia. These cells are found within the brain parenchyma, notably in the ventral/dorsal hippocampus CA1 *st rad* and *st lac mol*. Dark microglia exhibit several markers of cellular stress (dilatation of endoplasmic reticulum and Golgi, elongated mitochondria) as well as a dark, electron-dense cytoplasm and nucleoplasm [64]. These stressed microglia are rare in healthy mature mice, but become abundant in pathological conditions [64] including in a MIA mouse model induced with polyinosinic:polycytidulic acid (poly I:C) [49]. In the current study, we characterized the density and ultrastructure of dark microglia in the dorsal hippocampus CA1, *st rad* and *st lac mol*, comparing mHFD with CD offspring at P30. While imaging, we also noticed intriguing dark perivascular cells, localized inside the perivascular space yet displaying dark features similar to the dark microglia (i.e., dark, electron-dense cytoplasm and nucleoplasm, as well as markers of cellular stress). We further encountered apoptotic cells, identified by their dark cytoplasm, which was accompanied in this case by a distinctive pyknotic and fragmented nucleus. We decided to also quantify their density. The quantitative analysis of dark microglia and apoptotic cells revealed no significant difference in

their density among the *st rad* and *st lac mol* of the adolescent offspring, regardless of their sex and maternal diet (Supplementary Table 1; Fig. 7a-c). Notwithstanding, more than half of the apoptotic cells we observed (four out of seven) were identified as microglia by their IBA1^{+} staining. In the *st rad*, dark perivascular cells also displayed a similar density between offspring groups. In the *st lac mol*, however, a sex difference was observed, with the female offspring showing a significantly increased density of dark perivascular cells ($F_{(1,12)} = 5.692$, $p = 0.0344$) compared to male offspring (12.58 ± 1.99 cell/mm² *vs* 0.94 ± 0.94 cell/mm²) (Supplementary Table 1; Fig. 7d-e); regardless of maternal diet.

To study changes in organelles among the stressed dark cells in the *st lac mol*, we pooled together dark microglia and dark perivascular cells to obtain a sufficient sample size, required to be around 50 individual cells total for a large effect size (~ 0.4) (also see Supplementary Table 2 for the semi-descriptive analysis of the dark microglia and dark perivascular cells considered separately). This quantitative analysis of dark cells revealed a main diet effect on their number of dilated endoplasmic reticulum or Golgi apparatus cisternae, which significantly increased ($F_{(1,55)} = 4.264$, $p = 0.0437$) in mHFD compared to CD offspring (14.38 ± 0.62 dilated cisterna *vs* 9.805 ± 3.090 dilated cisterna) (Supplementary Table 3; Fig. 7f-j). In addition, secondary lysosomes were significantly more abundant in female offspring compared to male offspring regardless of their maternal diet (Female offspring: 0.453 ± 0.120 lysosomes *vs* Male offspring: 0.077 ± 0.109 lysosomes) (Supplementary Table 3). This finding may describe a sex difference, regardless of maternal diet, in terms of dark cells phagolysosomal pathways. Across groups, the two types of stressed dark cells lastly displayed in the *st lac mol* similar numbers of lysosomes, lipofuscin, endosomes and mitochondria, and their relationships with the microenvironment did not differ between groups.

Discussion

Our study investigated the effects of a fat enriched maternal diet on peripheral immune and microglial properties in the adolescent offspring of each sex. Characterization of our mouse model revealed a MIA phenotype defined by elevated circulating IL-6 in the mothers, together with increased fat deposition in the mothers and male offspring without other major metabolic changes. This MIA model led to peripheral immune priming demonstrated by exacerbated release of IL-6 upon a LPS-induced immune challenge in mHFD-exposed male and female offspring. The mHFD-induced MIA resulted in significant microglial morphological changes in the dorsal hippocampus CA1. We also found sexually dimorphic hippocampal transcriptomic changes, with mHFD-exposed male offspring showing reduced mRNA expression of the inflammatory-regulating cytokine *Tgf1b* and microglial receptors *Tmem119*, *Trem2* and *Cx3cr1*. In parallel to these changes, mHFD-exposed male offspring had increased microglial interactions with astrocytes in the dorsal hippocampus CA1, while both mHFD males and females had decreased microglia-associated extracellular space pockets in the same region. Taken together, this data highlights the emergence of a partially sex-dependent priming that lasted until adolescence in the mHFD offspring.

Previous work studying the metabolic consequences of mHFD in rodents have reported variable effects. With the same diet protocol that we used but in rats, Sasaki *et al*. observed that weight differences varied with the age of the offspring across their lifespan upon exposure to mHFD [13, 32]. mHFD offspring were significantly heavier during pubertal stages (P8-21) [13], while at adolescence (P35) [32] and adulthood (P90), their weight was similar to control animals [13]. Similarly, we did not find any significant difference of body weight in the P30 adolescent mouse offspring. By contrast, during early postnatal ages (P1 to P10), rat offspring exposed to lower fat mHFD (43% kCal/fat *vs* our 60% kCal/fat) became heavier with an increased fat mass [83], similar to our mHFD-exposed male offspring. In contrast to our observations, this study also reported heavier dams with lower blood glucose levels prior to mating [83], describing a diet-induced obesity model. Bilbo and Tsang compared two types of mHFD in rats –one with saturated fat and the other with trans-fat– with the same protocol duration used here, and found that both diets led to heavier dams [8]. In offspring, exposure to mHFD rich in saturated fats, and not trans-fats, led to significant weight grain in both sexes at puberty (P20) and in males at adulthood (P60) [8]. Overall, these studies suggest that the diet composition and exposure time may differently impact on the dams and offspring metabolism. In comparison, our mHFD mouse model did not result in severe endocrinologic alterations in the

dams thus suggesting that the effects observed in our offspring were primarily due to the immunologic consequences of a fat enriched diet during pregnancy and nurturing, without confounding endocrine risk factors.

Few studies have examined the MIA induced by mHFD as well as the mechanisms underlying these MIA effects of mHFD. Using a macaque model of mHFD, Thompson *et al*. have noted an elevation of the pro-inflammatory cytokine IL-12 and a decrease of macrophage-derived chemokine (also known as C-C motif chemokine 22) in the blood of the mothers [9]. This study was the first to directly highlight the interplay among metabolic and inflammatory maternal changes resulting from the diet and their consequences on the offspring behaviors. In rodents, Bilbo and Tsang did not observe an increase in IL-6 in rat dams fed with a high saturated fat diet [8], contrary to our study. However, subsequent studies using a mouse model as well as a more sensitive approach involving multiplex-ELISA observed increased levels of circulating cytokines, including IL-6, in dams, during pregnancy [68] and the end of nurturing [14]. Discrepancy between Bilbo and Tsang with ours' and others' results may be explained by the difference in the sensitivity between the techniques. In addition, differences between the diets or species used could also underlie this discrepancy. Interestingly, pregnant female rat fed with a HFD had increased mRNA levels of *Il-6* in the placenta [68], suggesting that IL-6 could cross the placental barrier to modulate fetal development [84] in our model.

In the mHFD-exposed offspring, alterations of the inflammatory status has notably been highlighted by increased cytokines levels (i.e. IL-5) in the blood of male mice at P7 and of female mice at P21 [14]. Moreover, another independent study has reported increased peripheral IL-6 four hours after a LPS immune challenge in adult rat male and female offspring [8]. In agreement with our results, these data suggest that during both adolescence and adulthood, mHFD-exposed offspring have a stronger response to a systemic immune challenge. IL-6 could contribute to inducing immune programming changes in the offspring by modifying transcriptional regulation of inflammatory mediators that are part of IL-6 downstream signaling target (i.e. *AP1*, *NFκB*, *Sp1*) [85]. It is also possible that a stronger response to immune challenge occurs through increased release of cytokines by fat deposits. In the homeostatic central nervous system, Bilbo and Tsang reported an increase of protein levels of IL-1β without change of mRNA levels of *Il-1β* and *Il-6* in P20 pubertal and P60 adult offspring, from both sexes [8]. Another group, Sasaki *et al*., revealed greater mRNA levels of *Il-6* in the adolescent hippocampus [32] and no difference compared to control in the adult hippocampus [13] using a similar diet protocol in male and female rats. In the present study, we did not detect *Il-1 β* or *Il-6* mRNA, suggesting levels below threshold for detection by rt-qPCR or a lower efficiency of the primers used. Although Sasaki *et al*. focused on an adolescent timepoint, they looked later, at P45. Therefore, it is plausible that the expression of inflammatory molecules –at protein and mRNA levels– varies between the two adolescent time points. It would be interesting to determine if adolescence represents a shifting or transition period for inflammatory signals, from a pubertal-like to an adult-like inflammatory phenotype.

In parallel to the changes of pro-inflammatory genes, neuroendocrine regulators genes (i.e. *Gr*, *Mr*, *Nfκb)* were also reported to be differently expressed in the rat hippocampus across adolescence and adulthood [13, 32, 86]. These neuroendocrine receptors can modulate microglial functions such as their release of inflammatory mediators (i.e. IL-1β, IL-6, TNF-α) during a LPS immune challenge [87–89], their morphology [90], cellular dynamics and proliferation [89]. Moreover, neuroendocrine receptors are differently expressed by microglia between the sexes [91]. In the current study we observed a sexual dimorphism of the inflammatory-regulating cytokine *Tgfb1*, with lower expression levels detected in whole hippocampus of mHFD-exposed male offspring compared to other offspring groups.

mHFD studies have mainly examined its effects on global inflammation and gene expression changes, without focusing on microglia. However, microglia may represent one of the key actors mediating the pathological consequences of mHFD during neurodevelopment. Bilbo and Tsang previously reported higher density of $IBA1^+$ cells in the hippocampus CA1, CA3 and dentate gyrus of mHFD-exposed male and female rat offspring at adulthood [8]. In the present study, we did not observe any change in microglial density in the *st rad* and *st lac mol* of the dorsal hippocampus CA1. This could be explained by the method of analysis where microglia are identified by integrated density of $IBA1^+$ staining among hippocampal regions (CA1, CA3, dentate gyrus) *vs* count of $IBA1^+/TMEM119^+$ cells in individual CA1 layers, together with

the age or the species of animals used. Nevertheless, we observed microglial morphological changes in the *st rad* (circularity) and in *st lac mol* (solidity), as well as a decreased average branch length in the *st lac mol*. The reduced microglial circularity in the *st rad* of mHFD-exposed offspring suggests that these cells took a more elongated shape. Microglia with an elongated, rod-like morphology have been previously proposed to play a role in the response to acute brain insults due to their increased prevalence [92]. Elongated bipolar microglia were also previously described in a viral MIA model, in which *ex vivo* analyses also revealed that microglial chemotaxis and phagocytosis are increased in response to treatment (chemotaxis: CCL-2, IL-8, phagocytosis: LPS, poly I:C) [93]. The increased microglial solidity may represent a change in the distribution of the arborization, particularly a decreased distance between branches which would reflect a more convex-like shape. Others also hypothesized that an increase of the solidity value occurs during the morphological shift from a ramified to an amoeboid shape upon neuroinflammatory insults, and represents a de-ramified or bushy morphology [94, 95], a phenotype seen upon exposure to stress [96]. In a bacterial MIA mouse model, microglia were previously shown to shift their morphology to an ameboid shape in adolescent (P40) offspring amygdala [97]. Although the microglial morphological changes we observed varied between layers, similarly they could indicate a general shift from a surveillant-ramified state to an amoeboid shape. This morphological shift may also accompany microglial functional alterations in the hippocampus CA1 of mHFD offspring.

Microglia from the mHFD *vs* CD offspring interacted differently with their microenvironment. In *st lac mol*, the presence of extracellular space pockets surrounding microglial cell bodies decreased, which could be explained by various mechanisms. For instance, changes in the composition of the extracellular matrix could lead to a global decrease in extracellular space [98]. Microglia themselves were shown to contribute to modifying the extracellular matrix by releasing proteases (e.g. cathepsins, heparinases, metalloproteinases) [99, 100] that can promote their cell body migration or process motility, notably in inflammatory contexts [99, 100] or during brain plasticity [36]. Indeed, during visual deprivation in juvenile mice, the pockets of extracellular space surrounding microglia were shown to undergo reorganization [36] that was hypothesized to promote microglia motility and/or even dendritic spine structural plasticity and pruning [36, 101]. Hence, the decrease of extracellular space pockets-associated with microglial cell bodies that we observed could indicate a decrease in their motility and synaptic pruning function necessary for proper neuronal network maturation, which could be examined using *ex vivo* or *in vivo* imaging [98, 102].

Furthermore, these morphological and functional changes were associated with a decreased expression of microglial receptors (i.e. *Cx3cr1*, *Tmem119*, *Trem2*) in adolescent male offspring. TMEM119 is a protein considered to be expressed constitutively and exclusively by microglia in the brain [50]. Although its role remains under investigation, TMEM119 is required for microglial survival [75]. The absence of changes in the size of the microglial and infiltrating myeloid cells populations suggest no major issue with microglia survival in the *st rad* and *st lac mol*. Nevertheless, it is plausible that the turnover rate of microglia may change in the mHFD-exposed male offspring without affecting the population at a given time point. In this case, future investigation should consider examining microglial density, but also proliferation and apoptosis. Further investigation into TMEM119 function would help to assess if this receptor is also involved in cell-cell interactions. Similar to TMEM119, TREM2 aids microglia to survive, in addition to mediating other functions including blood flow regulation [103], phagocytosis and synaptic pruning [76, 79–81]. CX3CR1 is also involved in phagocytosis and synaptic remodeling by microglia [77, 78, 104]. Hence, a decrease of *Cx3cr1* and *Trem2* mRNA expression may reflect reduced microglial interactions with neurons or synaptic elements as well as phagocytic activities, which was not observed at the ultrastructural level. It should be noted however that our ultrastructural analysis focused on microglial cell bodies, leaving the possibility that microglial processes make less contacts with synapses, which remains to be explored. Further investigation into the protein expression of *Cx3cr1* and *Trem2* is also required. While the exact signaling pathway or receptor involved in microglia-astrocyte crosstalk has not been ascertained, a recent study suggested that microglial TREM2 may be involved. Indeed, using a TREM2 knockout mouse model, TREM2 deficiency led to a lack of microglia-astrocyte interactions in the cerebral cortex and hippocampus, which prevented the astrocytic-mediated phagocytosis of axon terminals [105]. The decrease of TREM2 we observed may represent a partial loss of microglial control over this newly

defined function of astrocytes at synapses. Taken with the male-specific increase of microglial interactions with astrocytes that we observed in our ultrastructural analysis, these results stress the importance of determining the molecular crosstalk between microglia and astrocytes that is at play in mHFD-exposed male offspring. Characterization by *in vivo* imaging of astrocyte-axon terminals interactions while performing microglial modulation could allow to investigate the microglia-astrocyte-synapse relationships further.

Since transcriptomic analyses were performed on whole hippocampi, it remains possible that microglial survival, density and/or synaptic remodeling were altered in other regions and/or layers of the hippocampus beyond the CA1 *st rad* and *st lac mol*. Subsequent studies could characterize differences in other regions and layers, and also, how transcriptomic changes occur between sexes in the mHFD model. It would be important for instance to assess whether the mechanisms recruited in female involve differences in post-translational modifications and/or protein expression. Interestingly, Glendining and Jasoni investigated epigenetic changes of the oxytocin receptor in the hippocampus of mHFD-exposed male and female mouse offspring by chromatin immunoprecipitation-qPCR (ChIP-qPCR), which revealed a sexually dimorphic pattern of acetylation and methylation leading to an increased expression of the oxytocin receptor in male offspring only [106]. Further investigation looking at whole genome epigenomic changes could hence provide, in parallel with proteomic analysis, better understanding of how microglial gene expression differs between sexes upon mHFD.

Our laboratory has previously identified dark microglia as a subset of microglia associated with pathological conditions that are characterized by a dark cytoplasm and nucleoplasm without a clear chromatin pattern [49, 64]. Not only microglia can undertake a 'dark' appearance, but several other types of brain cells such as neurons, oligodendrocytes [53, 61] and astrocytes [107, 108] as well. Here, we not only observed dark microglia, but also stressed dark perivascular cells showing several signs of cellular stress (i.e. elongated mitochondria and dilated cisternae of the endoplasmic reticulum and Golgi apparatus) and dying apoptotic cells in the dorsal hippocampus CA1 of the P30 offspring. No difference in the density of stressed dark cells and apoptotic cells was observed with the maternal diet. However, an interesting observation we made was the increased density of stressed dark perivascular cells in the *st rad* of female offspring compared to male offspring from both maternal diets. Unfortunately, the low sample size of stressed dark cells and apoptotic cells did not allow us to perform quantitative analysis in the dorsal hippocampus CA1 *st rad*. Similar to previous observations by our team in adult pathological conditions, dark microglia were mainly found to be located in the *st lac mol* among the CA1 [64]. We thus assessed the global changes in stressed dark cells organelles without discriminating dark microglia from dark perivascular cells to increase our sample size. This analysis of dark microglia and dark perivascular cells revealed a significantly increased number of dilated endoplasmic reticulum and Golgi apparatus cisternae. Dilation of the endoplasmic reticulum and the Golgi apparatus are well characterized ultrastructural signs of oxidative stress [109]. The increase in their incidence thus reflects a higher level of cellular stress in the dorsal hippocampus CA1 of mHFD-exposed adolescent offspring. It would be interesting to investigate the cellular stress signature of the two cell types at the molecular level, and the effects of dark microglia as well as dark perivascular cells on the blood-brain barrier. In fact, increased stress within the neurovascular unit could alter blood-brain barrier integrity and permeability, as well as the regulation of blood flow. Consequently, a dysfunctional blood-brain barrier may leak into the brain peripheral inflammatory signals released upon mHFD, such as IL-6, thus contributing to the microglial changes observed.

Conclusion

Although mHFD induced similar phenotypes in both sexes for immune priming and microglial morphology, we identified sex-specific effects in the mHFD male offspring in terms of transcriptomic and functional ultrastructural changes during adolescence. Considering their key role in shaping brain neuronal networks, microglia in dorsal hippocampus may be partially responsible for several pathological neurodevelopmental outcomes described in mHFD models. Adolescence is a period of intense brain plasticity and maturation, where several microglia-mediated processes, such as synaptic pruning and myelination, are ongoing and may be profoundly impacted by the mHFD-driven microglial priming. Notably, synaptic pruning involving microglia-astrocyte crosstalk may be especially impacted negatively in mHFD-exposed male offspring.

Investigation into these specific neurodevelopmental processes across the brain and the kinetics of their alterations during the offspring neurodevelopment, from embryonic stages to young adulthood, will be central to understanding the sexually dimorphic pathological cascade involving microglia.

List Of Abbreviation

AP-1: activator protein-1

Aif1: allograft inflammatory factor 1

a.u.: arbitrary units

ANOVA: analysis of variance

CA: cornu ammonis

CD: control chow

cDNA: complementary deoxyribonucleic acid

Cx3cr1: fractalkine receptor

DAB: diaminobenzidine

E: embryonic day

ELISA: enzyme-linked immunosorbent assay

HFD: high-fat diet

IBA1: ionized calcium-binding adapter 1

IL: interleukin

Il1ra: IL1 receptor antagonist

IκB: Nfκb inhibitor

LPS: lipopolysaccharide

mHFD: maternal HFD

MIA: maternal immune activation

MKP-1: mitogen-activated kinase protein 1

mRNA: messenger RNA

Nfκb: nuclear factor κ-light-chain-enhancer activator of B cells)

P: postnatal day

PB: phosphate buffer

PBS: phosphate buffered saline

PFA: paraformaldehyde

RNA: ribonucleic acid

RPL32: ribosomal protein L32

Rt-qPCR: real-time quantitative polymerase chain reaction

SAL: saline

SEM: scanning electron microscopy

Sp-1: specificity protein 1

St lac mol: *stratum lacunosum moleculare*

St rad: *stratum radiatum*

TBS: tris buffered saline

Tgf1β R: Transforming growth factor beta 1 receptor

TMEM119: transmembrane protein 119

TNF: tumor necrosis factor

Trem2: triggering receptor expressed on myeloid cells 2

W: week

Declarations

Ethics approval and consent to participate

All animal protocols were approved by McGill's Facility Animal Care Committee under the ethical guidelines of the Canadian Council on Animal Care.

Consent for publication

Not applicable

Availability of data and materials

The data that support the findings of this study are available from the corresponding author, MET, upon reasonable request.

Competing interests

Not applicable

Funding

This research was supported by an NSERC Discovery grant awarded to MET (#RGPIN-2014-05308). MB is a holder of the FRQS doctoral award. During the study, CL received the Returning student award from the Integrated Program in Neuroscience of McGill University, and LFC held the Vanier Canada Graduate scholarship. JCS received the FRQS postdoctoral fellowship. FGI is a holder of a full doctoral scholarship from CONTACYT, Mexican Council of Science and Technology. MET is a Canada Research Chair (Tier II) in *Neurobiology of Aging and Cognition*.

Authors' contributions

MB designed the initial experiments and coordinated most of the experiments. CL and NV helped with the optimization of RNA isolation and, NV gave precious guidance for rt-qPCR design and taught MB electron microscopy tissue processing. JCS helped with experimental design for ultrastructural imaging and analysis using SEM. MET provided constructive insights into experimental design and data interpretation throughout the study.

MB performed and analyzed all the physiological follow-ups of the pregnant mothers and offspring as well as multiplex-ELISA on the mothers. MB mainly performed tissue processing, and all data analyses. CL and LFC assisted with part of the animal care, the sacrifice of the offspring and performed multiplex-ELISA experiments on the offspring. CL and LFC discussed possible avenue to better answer the experimental questions of this study. JCS and FGI provided their expertise and imaged for ultrastructural analysis using SEM.

MB mainly wrote the manuscript under guidance from MET. All authors read, edited and approved the final manuscript.

Acknowledgements

We are grateful to Julie-Christine Lévesque for providing training and support at the Bioimaging platform of the *Infectious Disease Research Center* funded by the Canadian Foundation Innovation (CFI) and Dr Sebastien Hébert for the access to rt-qPCR apparatus. Warm thank to Katherine Picard and Marie-Kim St-Pierre who performed the confocal imaging for the morphological analyses of microglia. We are thankful to their positive energy and support throughout this study. We also thank Iris Kim and Kasia J. Szyszkowicz for technical support. Finally, we are thankful to Giamal N. Luheshi for help providing animals and support with the first part of these experiments and Mallar Chakravarty for his guidance and support towards the end of the study.

References

1. Bolton JL, Bilbo SD. Developmental programming of brain and behavior by perinatal diet: focus on inflammatory mechanisms. Dialogues Clin Neurosci. 2014;16:307–20.
2. Sullivan EL, Riper KM, Lockard R, Valleau JC. Maternal High-Fat Diet Programming of the Neuroendocrine System and Behavior. Horm Behav. 2015;76:153–61.
3. Mina TH, Lahti M, Drake AJ, Räikkönen K, Minnis H, Denison FC, et al. Prenatal exposure to very severe maternal obesity is associated with adverse neuropsychiatric outcomes in children. Psychol Med. 2017;47:353–62.
4. Chen C, Xu X, Yan Y. Estimated global overweight and obesity burden in pregnant women based on panel data model. PLoS ONE. 2018;13:e0202183.
5. Bleich SN, Cutler D, Murray C, Adams A. Why Is the Developed World Obese? Annu Rev Public Health. 2008;29:273–95.
6. Hariri N, Thibault L. High-fat diet-induced obesity in animal models. Nutr Res Rev. 2010;23:270–99.
7. Sauerwald TU, Demmelmair H, Koletzko B. Polyunsaturated fatty acid supply with human milk. Lipids. 2001;36:991–6.
8. Bilbo SD, Tsang V. Enduring consequences of maternal obesity for brain inflammation and behavior of offspring. FASEB J. 2010;24:2104–15.

9. Thompson JR, Gustafsson HC, DeCapo M, Takahashi DL, Bagley JL, Dean TA, et al. Maternal Diet, Metabolic State, and Inflammatory Response Exert Unique and Long-Lasting Influences on Offspring Behavior in Non-Human Primates. Front Endocrinol. 2018;9:161.
10. Winther G, Elfving B, Müller HK, Lund S, Wegener G. Maternal High-fat Diet Programs Offspring Emotional Behavior in Adulthood. Neuroscience. 2018;388:87–101.
11. Sullivan EL, Grayson B, Takahashi D, Robertson N, Maier A, Bethea CL, et al. Chronic Consumption of a High-Fat Diet during Pregnancy Causes Perturbations in the Serotonergic System and Increased Anxiety-Like Behavior in Nonhuman Primate Offspring. J Neurosci. 2010;30:3826–30.
12. Peleg-Raibstein D, Luca E, Wolfrum C. Maternal high-fat diet in mice programs emotional behavior in adulthood. Behav Brain Res. 2012;233:398–404.
13. Sasaki A, de Vega WC, St-Cyr S, Pan P, McGowan PO. Perinatal high fat diet alters glucocorticoid signaling and anxiety behavior in adulthood. Neuroscience. 2013;240:1–12.
14. Graf AE, Lallier SW, Waidyaratne G, Thompson MD, Tipple TE, Hester ME, et al. Maternal high fat diet exposure is associated with increased hepcidin levels, decreased myelination, and neurobehavioral changes in male offspring. Brain Behav Immun. 2016;58:369–78.
15. Cordner ZA, Khambadkone SG, Boersma GJ, Song L, Summers TN, Moran TH, et al. Maternal high-fat diet results in cognitive impairment and hippocampal gene expression changes in rat offspring. Exp Neurol. 2019;318:92.
16. Tozuka Y, Kumon M, Wada E, Onodera M, Mochizuki H, Wada K. Maternal obesity impairs hippocampal BDNF production and spatial learning performance in young mouse offspring. Neurochem Int. 2010;57:235–47.
17. Grissom NM, Herdt CT, Desilets J, Lidsky-Everson J, Reyes TM. Dissociable Deficits of Executive Function Caused by Gestational Adversity are Linked to Specific Transcriptional Changes in the Prefrontal Cortex. Neuropsychopharmacology. 2015;40:1353–63.
18. Smith BL, Laaker CJ, Lloyd KR, Hiltz AR, Reyes TM. Adolescent microglia play a role in executive function in male mice exposed to perinatal high fat diet. Brain Behav Immun [Internet]. 2019 [cited 2019 Nov 26]; Available from: http://www.sciencedirect.com/science/article/pii/S0889159119306312.
19. Meyer U, Feldon J, Fatemi SH. In-vivo rodent models for the experimental investigation of prenatal immune activation effects in neurodevelopmental brain disorders. Neurosci Biobehav Rev. 2009;33:1061–79.
20. Estes ML, McAllister AK. Maternal immune activation: implications for neuropsychiatric disorders. Science. 2016;353:772–7.
21. Brucato M, Ladd-Acosta C, Li M, Caruso D, Hong X, Kaczaniuk J, et al. Prenatal exposure to fever is associated with Autism Spectrum Disorder in the Boston Birth Cohort. Autism Res Off J Int Soc Autism Res. 2017;10:1878–90.
22. Bilbo SD, Block CL, Bolton JL, Hanamsagar R, Tran PK. Beyond infection - Maternal immune activation by environmental factors, microglial development, and relevance for autism spectrum disorders. Exp Neurol. 2018;299:241–51.
23. Feigenson KA, Kusnecov AW, Silverstein SM. Inflammation and the Two-Hit Hypothesis of Schizophrenia. Neurosci Biobehav Rev. 2014;38:72–93.
24. Delpech J-C, Wei L, Hao J, Yu X, Madore C, Butovsky O, et al. Early life stress perturbs the maturation of microglia in the developing hippocampus. Brain Behav Immun. 2016;57:79–93.
25. Rincel M, Lépinay AL, Janthakhin Y, Soudain G, Yvon S, Silva SD, et al. Maternal high-fat diet and early life stress differentially modulate spine density and dendritic morphology in the medial prefrontal cortex of juvenile and adult rats. Brain Struct Funct. 2017;1–13.
26. Huizink AC, Mulder EJH. Maternal smoking, drinking or cannabis use during pregnancy and neurobehavioral and cognitive functioning in human offspring. Neurosci Biobehav Rev. 2006;30:24–41.

27. Proietti E, Röösli M, Frey U, Latzin P. Air Pollution During Pregnancy and Neonatal Outcome: A Review. J Aerosol Med Pulm Drug Deliv. 2012;26:9–23.
28. Bolton JL, Auten RL, Bilbo SD. Prenatal air pollution exposure induces sexually dimorphic fetal programming of metabolic and neuroinflammatory outcomes in adult offspring. Brain Behav Immun. 2014;37:30–44.
29. Knuesel I, Chicha L, Britschgi M, Schobel SA, Bodmer M, Hellings JA, et al. Maternal immune activation and abnormal brain development across CNS disorders. Nat Rev Neurol. 2014;10:643–60.
30. Trépanier MO, Hopperton KE, Mizrahi R, Mechawar N, Bazinet RP. Postmortem evidence of cerebral inflammation in schizophrenia: a systematic review. Mol Psychiatry. 2016;21:1009–26.
31. van Kesteren CFMG, Gremmels H, de Witte LD, Hol EM, Van Gool AR, Falkai PG, et al. Immune involvement in the pathogenesis of schizophrenia: a meta-analysis on postmortem brain studies. Transl Psychiatry. 2017;7:e1075.
32. Sasaki A, de Vega W, Sivanathan S, St-Cyr S, McGowan PO. Maternal high-fat diet alters anxiety behavior and glucocorticoid signaling in adolescent offspring. Neuroscience. 2014;272:92–101.
33. Schwarz JM, Bilbo SD. Sex, Glia, and Development: interactions in health and disease. Horm Behav. 2012;62:243–53.
34. Hanamsagar R, Bilbo SD. Sex differences in neurodevelopmental and neurodegenerative disorders: Focus on microglial function and neuroinflammation during development. J Steroid Biochem Mol Biol. 2016;160:127–33.
35. Bordeleau M, Carrier M, Luheshi GN, Tremblay M-È. Microglia along sex lines: From brain colonization, maturation and function, to implication in neurodevelopmental disorders. Semin Cell Dev Biol. 2019;94:152–63.
36. Tremblay M-È, Lowery RL, Majewska AK. Microglial Interactions with Synapses Are Modulated by Visual Experience. PLOS Biol. 2010;8:e1000527.
37. Domingues HS, Portugal CC, Socodato R, Relvas JB. Oligodendrocyte, Astrocyte, and Microglia Crosstalk in Myelin Development, Damage, and Repair. Front Cell Dev Biol. 2016;4:71.
38. Kaur C, Rathnasamy G, Ling E-A. Biology of Microglia in the Developing Brain. J Neuropathol Exp Neurol. 2017;76:736–53.
39. Paolicelli RC, Ferretti MT. Function and Dysfunction of Microglia during Brain Development: Consequences for Synapses and Neural Circuits. Front Synaptic Neurosci. 2017;9:9.
40. Hatanaka Y, Wada K, Kabuta T. Maternal high-fat diet leads to persistent synaptic instability in mouse offspring via oxidative stress during lactation. Neurochem Int. 2016;97:99–108.
41. Paradis J, Boureau P, Moyon T, Nicklaus S, Parnet P, Paillé V. Perinatal Western Diet Consumption Leads to Profound Plasticity and GABAergic Phenotype Changes within Hypothalamus and Reward Pathway from Birth to Sexual Maturity in Rat. Front Endocrinol. 2017;8:216.
42. Janthakhin Y, Rincel M, Costa A-M, Darnaudéry M, Ferreira G. Maternal high-fat diet leads to hippocampal and amygdala dendritic remodeling in adult male offspring. Psychoneuroendocrinology. 2017;83:49–57.
43. Norden DM, Muccigrosso MM, Godbout JP. Microglial Priming and Enhanced Reactivity to Secondary Insult in Aging, and Traumatic CNS injury, and Neurodegenerative Disease. Neuropharmacology. 2015;96:29–41.
44. Bilbo SD, Schwarz JM. Early-Life Programming of Later-Life Brain and Behavior: A Critical Role for the Immune System. Front Behav Neurosci [Internet]. 2009 [cited 2020 Apr 21];3. Available from: https://www.ncbi.nlm.nih.gov/pmc/articles/PMC2737431/.
45. Yoon T, Okada J, Jung MW, Kim JJ. Prefrontal cortex and hippocampus subserve different components of working memory in rats. Learn Mem. 2008;15:97–105.
46. Lee A-R, Kim J-H, Cho E, Kim M, Park M. Dorsal and Ventral Hippocampus Differentiate in Functional Pathways and Differentially Associate with Neurological Disease-Related Genes during Postnatal Development. Front Mol Neurosci. 2017;10:331.

47. McHugh SB, Campbell TG, Taylor AM, Rawlins JNP, Bannerman DM. A Role for Dorsal and Ventral Hippocampus in Inter-Temporal Choice Cost-Benefit Decision Making. Behav Neurosci. 2008;122:1–8.
48. Spear LP. The adolescent brain and age-related behavioral manifestations. Neurosci Biobehav Rev. 2000;24:417–63.
49. Hui CW, St-Pierre A, El Hajj H, Remy Y, Hébert SS, Luheshi GN, et al. Prenatal Immune Challenge in Mice Leads to Partly Sex-Dependent Behavioral, Microglial, and Molecular Abnormalities Associated with Schizophrenia. Front Mol Neurosci [Internet]. 2018 [cited 2018 Mar 29];11. Available from: https://www.ncbi.nlm.nih.gov/pmc/articles/PMC5809492/.
50. Bennett ML, Bennett FC, Liddelow SA, Ajami B, Zamanian JL, Fernhoff NB, et al. New tools for studying microglia in the mouse and human CNS. Proc Natl Acad Sci U S A. 2016;113:E1738–46.
51. Ibanez González F, Picard K, Bordelau M, Sharma K, Bisht K, Tremblay M-È. Immunofluorescence Staining Using IBA1 and TMEM119 for Microglial Density, Morphology and Peripheral Myeloid Cell Infiltration Analysis in Mouse Brain. JoVE J Vis Exp. 2019;e60510.
52. Paxinos G, Franklin KBJ. Paxinos and Franklin's the mouse brain in stereotaxic coordinates. 4th ed. Amsterdam: Elsevier/Academic Press; 2013.
53. Tremblay M-È, Zettel ML, Ison JR, Allen PD, Majewska AK. Effects of aging and sensory loss on glial cells in mouse visual and auditory cortices. Glia. 2012;60:541–58.
54. Young K, Morrison H. Quantifying Microglia Morphology from Photomicrographs of Immunohistochemistry Prepared Tissue Using ImageJ. JoVE J Vis Exp. 2018;e57648.
55. St-Pierre M-K, Bordeleau M, Tremblay M-È. Visualizing Dark Microglia. Microglia. New York: Humana; 2019. pp. 97–110.
56. Hajj HE, Savage JC, Bisht K, Parent M, Vallières L, Rivest S, et al. Ultrastructural evidence of microglial heterogeneity in Alzheimer's disease amyloid pathology. J Neuroinflammation [Internet]. BioMed Central; 2019 [cited 2020 Apr 13];16. Available from: https://www.ncbi.nlm.nih.gov/pmc/articles/PMC6469225/.
57. Chavez-Valdez R, Flock DL, Martin LJ, Northington FJ. Endoplasmic Reticulum pathology and stress response in neurons precede programmed necrosis after neonatal hypoxia-ischemia. Int J Dev Neurosci Off J Int Soc Dev Neurosci NIH Public Access. 2016;48:58.
58. De Duve C. The lysosome. Sci Am. 1963;208:64–72.
59. Holtzman E, Novikoff AB, Villaverde H. LYSOSOMES, AND GERL IN NORMAL AND CHROMATOLYTIC NEURONS OF THE RAT GANGLION NODOSUM. J Cell Biol. 1967;33:419–35.
60. Nandy K. Properties of neuronal lipofuscin pigment in mice. Acta Neuropathol (Berl). 1971;19:25–32.
61. Peters A, Palay SL, Webster HdeF. The Fine Structure of the Nervous System. Neurons and their Supporting Cells. 3rd edition. J Neuropathol Exp Neurol. 1991;50:282–282.
62. Maxfield FR, Barbosa-Lorenzi VC, Singh RK. Digestive exophagy: Phagocyte digestion of objects too large for phagocytosis. Traffic. 2020;21:6–12.
63. Haka AS, Barbosa-Lorenzi VC, Lee HJ, Falcone DJ, Hudis CA, Dannenberg AJ, et al. Exocytosis of macrophage lysosomes leads to digestion of apoptotic adipocytes and foam cell formation. J Lipid Res. 2016;57:980–92.
64. Bisht K, Sharma KP, Lecours C, Gabriela Sánchez M, El Hajj H, Milior G, et al. Dark microglia: A new phenotype predominantly associated with pathological states. Glia. 2016;64:826–39.
65. Zhang J, Reedy MC, Hannun YA, Obeid LM. Inhibition of Caspases Inhibits the Release of Apoptotic Bodies: Bcl-2 Inhibits the Initiation of Formation of Apoptotic Bodies in Chemotherapeutic Agent-induced Apoptosis. J Cell Biol. 1999;145:99–108.
66. Faul F, Erdfelder E, Lang A-G, Buchner A. G*Power 3: a flexible statistical power analysis program for the social, behavioral, and biomedical sciences. Behav Res Methods. 2007;39:175–91.

67. Castanon N, Luheshi G, Layé S. Role of neuroinflammation in the emotional and cognitive alterations displayed by animal models of obesity. Front Neurosci [Internet]. 2015 [cited 2020 Feb 3];9. Available from: https://www.ncbi.nlm.nih.gov/pmc/articles/PMC4490252/.
68. Kretschmer T, Schulze-Edinghausen M, Turnwald E-M, Janoschek R, Bae-Gartz I, Zentis P, et al. Effect of Maternal Obesity in Mice on IL-6 Levels and Placental Endothelial Cell Homeostasis. Nutrients. 2020;12:296.
69. Ohta T, Toriniwa Y, Ryumon N, Inaba N, Hirao T, Yamanaka S, et al. Maternal high-fat diet promotes onset of diabetes in rat offspring. Anim Sci J. 2017;88:149–55.
70. Hohos NM, Skaznik-Wikiel ME. High-Fat Diet and Female Fertility. Endocrinology. 2017;158:2407–19.
71. Skelly DT, Hennessy E, Dansereau M-A, Cunningham C. A Systematic Analysis of the Peripheral and CNS Effects of Systemic LPS, IL-1B, TNF-α and IL-6 Challenges in C57BL/6 Mice. PLoS ONE [Internet]. 2013 [cited 2020 Feb 17];8. Available from: https://www.ncbi.nlm.nih.gov/pmc/articles/PMC3698075/.
72. Niraula A, Sheridan JF, Godbout JP. Microglia Priming with Aging and Stress. Neuropsychopharmacology. 2017;42:318–33.
73. Butovsky O, Jedrychowski MP, Moore CS, Cialic R, Lanser AJ, Gabriely G, et al. Identification of a Unique TGF-β Dependent Molecular and Functional Signature in Microglia. Nat Neurosci. 2014;17:131–43.
74. Kishikawa S, Sato S, Kaneto S, Uchino S, Kohsaka S, Nakamura S, et al. Allograft inflammatory factor 1 is a regulator of transcytosis in M cells. Nat Commun. 2017;8:1–10.
75. Zheng H, Jia L, Liu C-C, Rong Z, Zhong L, Yang L, et al. TREM2 Promotes Microglial Survival by Activating Wnt/β-Catenin Pathway. J Neurosci. 2017;37:1772–84.
76. Filipello F, Morini R, Corradini I, Zerbi V, Canzi A, Michalski B, et al. The Microglial Innate Immune Receptor TREM2 Is Required for Synapse Elimination and Normal Brain Connectivity. Immunity. 2018;48:979–91.e8.
77. Zhan Y, Paolicelli RC, Sforazzini F, Weinhard L, Bolasco G, Pagani F, et al. Deficient neuron-microglia signaling results in impaired functional brain connectivity and social behavior. Nat Neurosci. 2014;17:400–6.
78. Paolicelli RC, Bolasco G, Pagani F, Maggi L, Scianni M, Panzanelli P, et al. Synaptic Pruning by Microglia Is Necessary for Normal Brain Development. Science. 2011;333:1456–8.
79. Kawabori M, Kacimi R, Kauppinen T, Calosing C, Kim JY, Hsieh CL, et al. Triggering Receptor Expressed on Myeloid Cells 2 (TREM2) Deficiency Attenuates Phagocytic Activities of Microglia and Exacerbates Ischemic Damage in Experimental Stroke. J Neurosci. 2015;35:3384–96.
80. Chertoff M, Shrivastava K, Gonzalez B, Acarin L, Giménez-Llort L. Differential Modulation of TREM2 Protein during Postnatal Brain Development in Mice. PLOS ONE. 2013;8:e72083.
81. Thrash JC, Torbett BE, Carson MJ. Developmental regulation of TREM2 and DAP12 expression in the murine CNS: implications for Nasu-Hakola disease. Neurochem Res. 2009;34:38–45.
82. Schaefers ATU, Grafen K, Teuchert-Noodt G, Winter Y. Synaptic Remodeling in the Dentate Gyrus, CA3, CA1, Subiculum, and Entorhinal Cortex of Mice: Effects of Deprived Rearing and Voluntary Running. Neural Plast. 2010;2010:870573.
83. Barrand S, Crowley TM, Wood-Bradley RJ, Jong KAD, Armitage JA. Impact of maternal high fat diet on hypothalamic transcriptome in neonatal Sprague Dawley rats. PLOS ONE. 2017;12:e0189492.
84. Dahlgren J, Samuelsson A-M, Jansson T, Holmäng A. Interleukin-6 in the Maternal Circulation Reaches the Rat Fetus in Mid-gestation. Pediatr Res Nature Publishing Group. 2006;60:147–51.
85. Luo Y, Zheng SG. Hall of Fame among Pro-inflammatory Cytokines: Interleukin-6 Gene and Its Transcriptional Regulation Mechanisms. Front Immunol [Internet]. Frontiers; 2016 [cited 2020 Apr 17];7. Available from: https://www.frontiersin.org/articles/10.3389/fimmu.2016.00604/full.
86. Wijenayake S, Rahman MF, Lum CMW, Vega WCD, Sasaki A, McGowan PO. Maternal high-fat diet induces sex-specific effects on inflammatory responses to corticosterone and lipopolysaccharide challenge in adult rat offspring. bioRxiv. 2019;780783.

87. Barrientos RM, Thompson VM, Kitt MM, Amat J, Hale MW, Frank MG, et al. Greater Glucocorticoid Receptor Activation in Hippocampus of Aged Rats Sensitizes Microglia. Neurobiol Aging. 2015;36:1483–95.
88. Chantong B, Kratschmar DV, Nashev LG, Balazs Z, Odermatt A. Mineralocorticoid and glucocorticoid receptors differentially regulate NF-kappaB activity and pro-inflammatory cytokine production in murine BV-2 microglial cells. J Neuroinflammation. 2012;9:260.
89. Carrillo-de Sauvage M, Maatouk L, Arnoux I, Pasco M, Sanz Diez A, Delahaye M, et al. Potent and multiple regulatory actions of microglial glucocorticoid receptors during CNS inflammation. Cell Death Differ. 2013;20:1546–57.
90. van Olst L, Bielefeld P, Fitzsimons CP, de Vries HE, Schouten M. Glucocorticoid-mediated modulation of morphological changes associated with aging in microglia. Aging Cell [Internet]. 2018 [cited 2020 Apr 17];17. Available from: https://www.ncbi.nlm.nih.gov/pmc/articles/PMC6052476/.
91. Villa A, Gelosa P, Castiglioni L, Cimino M, Rizzi N, Pepe G, et al. Sex-Specific Features of Microglia from Adult Mice. Cell Rep. 2018;23:3501–11.
92. Taylor SE, Morganti-Kossmann C, Lifshitz J, Ziebell JM. Rod Microglia: A Morphological Definition. PLOS ONE Public Library of Science. 2014;9:e97096.
93. Ji P, Schachtschneider KM, Schook LB, Walker FR, Johnson RW. Peripheral Viral Infection Induced Microglial Sensome Genes and Enhanced Microglial Cell Activity in the Hippocampus of Neonatal Piglets. Brain Behav Immun. 2016;54:243–51.
94. Fernández-Arjona M, del M, Grondona, Fernández-Llebrez JM, López-Ávalos P MD. Microglial Morphometric Parameters Correlate With the Expression Level of IL-1β, and Allow Identifying Different Activated Morphotypes. Front Cell Neurosci [Internet]. Frontiers; 2019 [cited 2020 Apr 13];13. Available from: https://www.frontiersin.org/articles/10.3389/fncel.2019.00472/full.
95. Zanier ER, Fumagalli S, Perego C, Pischiutta F, De Simoni M-G. Shape descriptors of the “never resting” microglia in three different acute brain injury models in mice. Intensive Care Med Exp [Internet]. 2015 [cited 2020 Apr 13];3. Available from: https://www.ncbi.nlm.nih.gov/pmc/articles/PMC4513020/.
96. Tay TL, Béchade C, D’Andrea I, St-Pierre M-K, Henry MS, Roumier A, et al. Microglia Gone Rogue: Impacts on Psychiatric Disorders across the Lifespan. Front Mol Neurosci [Internet]. 2018 [cited 2018 Mar 21];10. Available from: https://www.ncbi.nlm.nih.gov/pmc/articles/PMC5758507/.
97. O’Loughlin E, Pakan JMP, Yilmazer-Hanke D, McDermott KW. Acute in utero exposure to lipopolysaccharide induces inflammation in the pre- and postnatal brain and alters the glial cytoarchitecture in the developing amygdala. J Neuroinflammation. 2017;14:212.
98. Hrabetova S, Cognet L, Rusakov DA, Nägerl UV. Unveiling the Extracellular Space of the Brain: From Super-resolved Microstructure to In Vivo Function. J Neurosci Society for Neuroscience. 2018;38:9355–63.
99. del Zoppo Gregory J, Richard M, Takuma M, Stephanie H, Xiaoyun W, Berg Greta I, et al. Microglial Activation and Matrix Protease Generation During Focal Cerebral Ischemia. Stroke American Heart Association. 2007;38:646–51.
100. Lively S, Schlichter LC. The microglial activation state regulates migration and roles of matrix-dissolving enzymes for invasion. J Neuroinflammation. 2013;10:843.
101. Tremblay M-È, Majewska AK. A role for microglia in synaptic plasticity? Commun Integr Biol. 2011;4:220–2.
102. Tønnesen J, Inavalli VVGK, Nägerl UV. Super-Resolution Imaging of the Extracellular Space in Living Brain Tissue. Cell. 2018;172:1108–21.e15.
103. Kleinberger G, Brendel M, Mracsko E, Wefers B, Groeneweg L, Xiang X, et al. The FTD-like syndrome causing TREM2 T66M mutation impairs microglia function, brain perfusion, and glucose metabolism. EMBO J. 2017;36:1837–53.
104. Noda M, Doi Y, Liang J, Kawanokuchi J, Sonobe Y, Takeuchi H, et al. Fractalkine Attenuates Excito-neurotoxicity via Microglial Clearance of Damaged Neurons and Antioxidant Enzyme Heme Oxygenase-1 Expression. J Biol Chem. 2011;286:2308–19.

105. Jay TR, Saucken VE von, Muñoz B, Codocedo JF, Atwood BK, Lamb BT, et al. TREM2 is required for microglial instruction of astrocytic synaptic engulfment in neurodevelopment. Glia. 2019;67:1873–92.
106. Glendining KA, Jasoni CL. Maternal High Fat Diet-Induced Obesity Modifies Histone Binding and Expression of Oxtr in Offspring Hippocampus in a Sex-Specific Manner. Int J Mol Sci [Internet]. 2019 [cited 2020 Feb 23];20. Available from: https://www.ncbi.nlm.nih.gov/pmc/articles/PMC6359595/.
107. Mori S, Leblond CP. Electron microscopic features and proliferation of astrocytes in the corpus callosum of the rat. J Comp Neurol. 1969;137:197–225.
108. Castejón OJ. Astrocyte subtypes in the gray matter of injured human cerebral cortex: a transmission electron microscope study. Brain Inj. Taylor & Francis; 1999;13:291–304.
109. Schönthal AH. Endoplasmic Reticulum Stress: Its Role in Disease and Novel Prospects for Therapy. Scientifica. 2012;2012:857516.
110. Grant CW, Moran-Paul CM, Duclos SK, Guberski DL, Arreaza-Rubín G, Spain LM. Testing Agents for Prevention or Reversal of Type 1 Diabetes in Rodents. PLOS ONE. 2013;8:e72989.

Figures

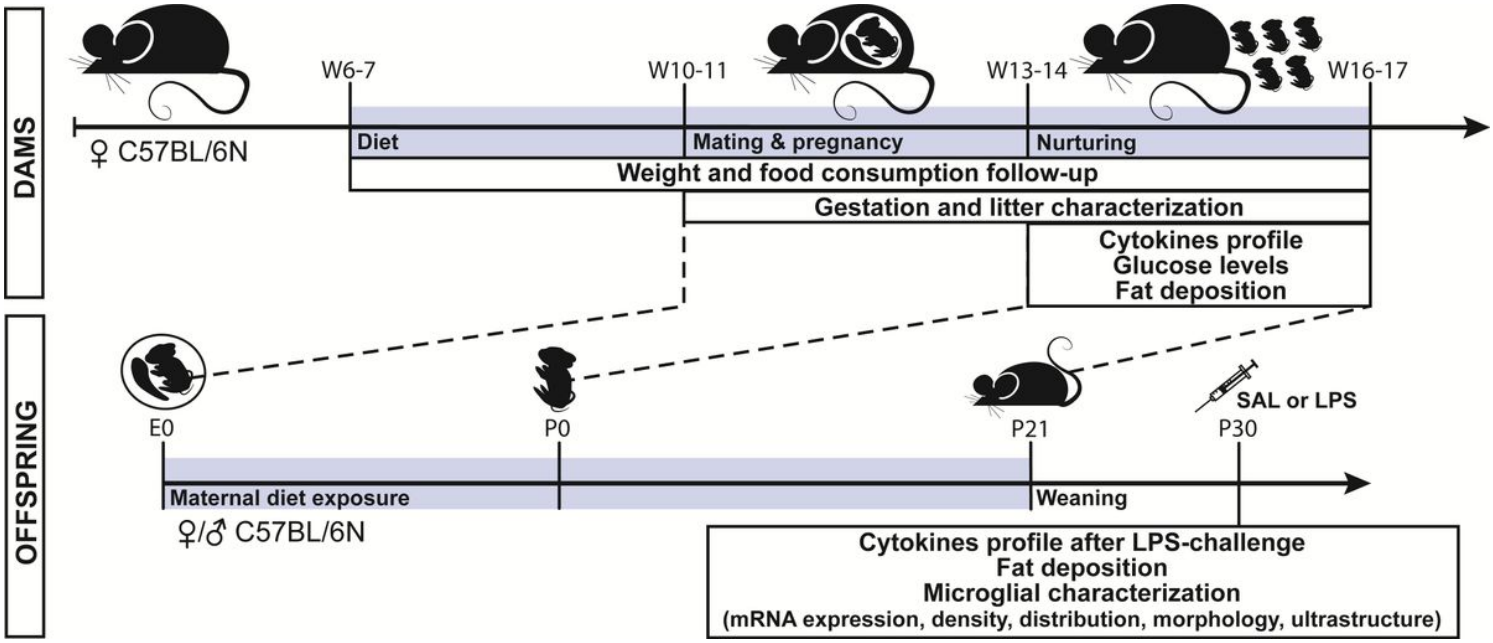

Figure 1

Experimental outline of HFD protocol on the dams and the offspring. Diet protocol period is identified by a pale blue-colored bar on the dams and the offspring timelines. At P21, all offspring were on normal chow diet before sacrifice at P30. Part of the animals received an intraperitoneal LPS injection 8 hours before characterizing their peripheral inflammatory profile. ♀: female, ♂: male, E: embryonic days, LPS: lipopolysaccharide, P: postnatal days, SAL: saline, W: weeks.

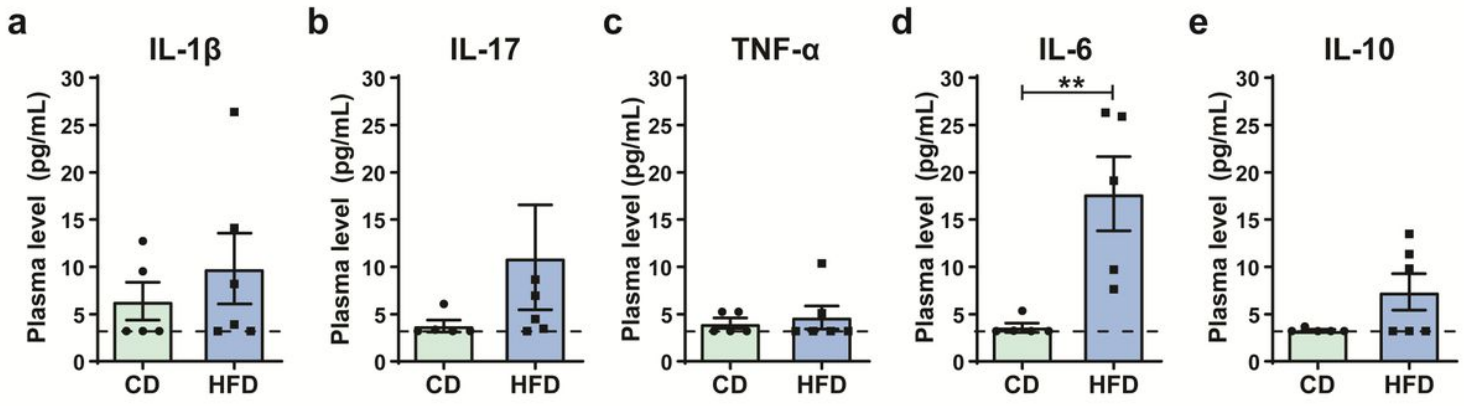

Figure 2

HFD effect on peripheral inflammatory profile in the dams at weaning of their litters. Plasma levels was measured by multiplex-ELISA for (a) IL-1 β, (b) IL-17, (c) TNF-α, (d) IL-6 and (e) IL-10. Detection limit of each graphs is represented by a dotted line. Data are shown as mean ± standard error of the mean. $p<0.01$, $p<0.01$** by Mann-Whitney test. CD: control diet, HFD: high-fat diet, IL: interleukin, TNF-α: tumor necrosis factor α.

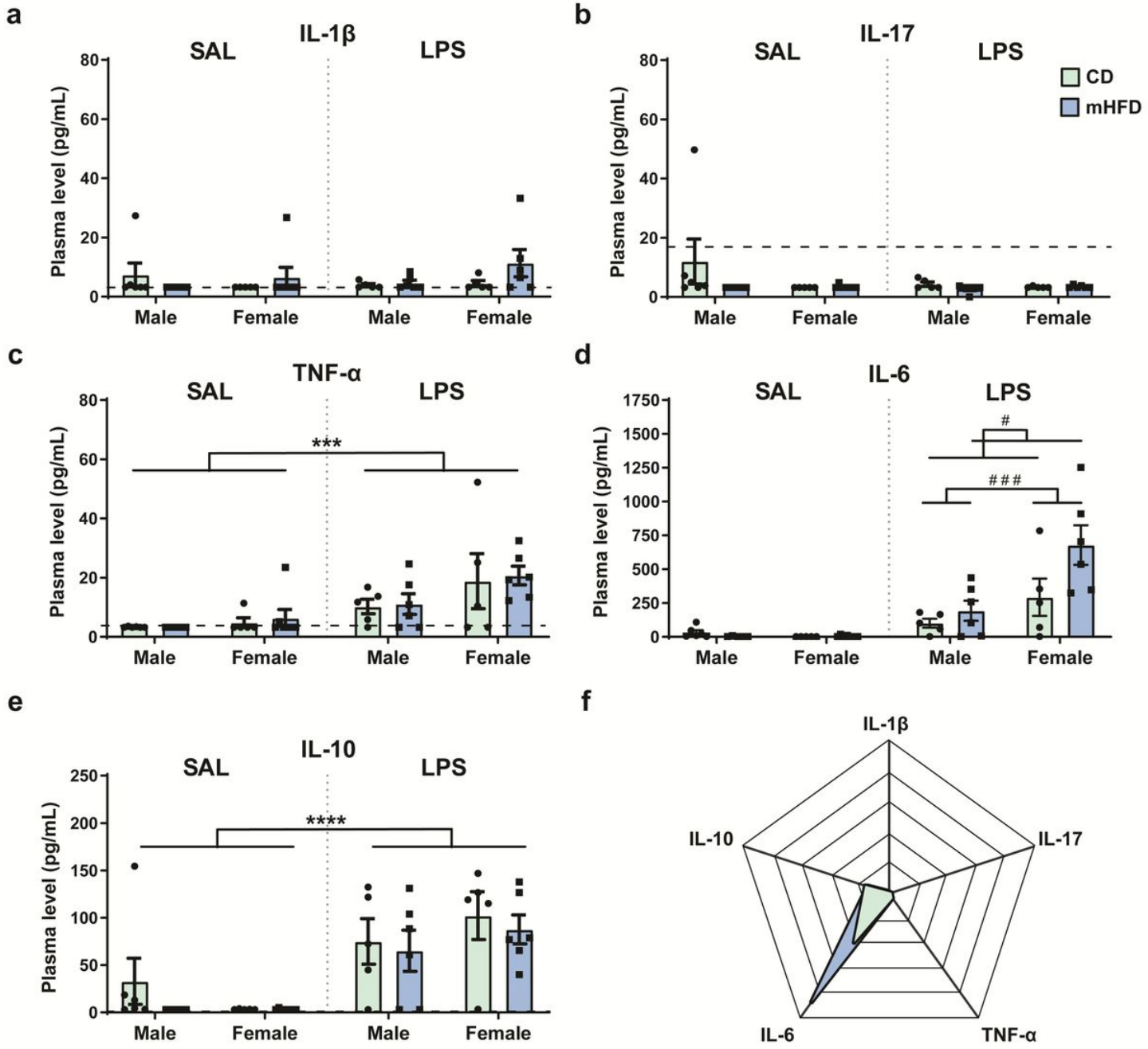

Figure 3

mHFD effect on plasma cytokine profile of P30 offspring eight hours after LPS treatment. (a) IL-1β, (b) IL-17, (c) TNF-α, (d) IL-6 and (e) IL-10 were measured by multiplex-ELISA in offspring plasma after administration of SAL or LPS by intraperitoneal injection. Dotted line on the graphs indicates the detection limits. (f) Radar graph illustrates cytokines levels in offspring from both diet groups regardless of their sex eight hours after LPS immune challenge. Data are shown as mean ± standard error of the mean. $p<0.001$***, $p<0.0001$**** (treatment) by mixed-effects analysis , $p<0.05$ # (treatment*diet), $p<0.01$ # # # (treatment*sex) by mixed-effects analysis. CD: control, LPS: lipopolysaccharide, IL: interleukin, SAL: saline, mHFD: maternal high-fat diet, TNF-α: tumor necrosis factor α.

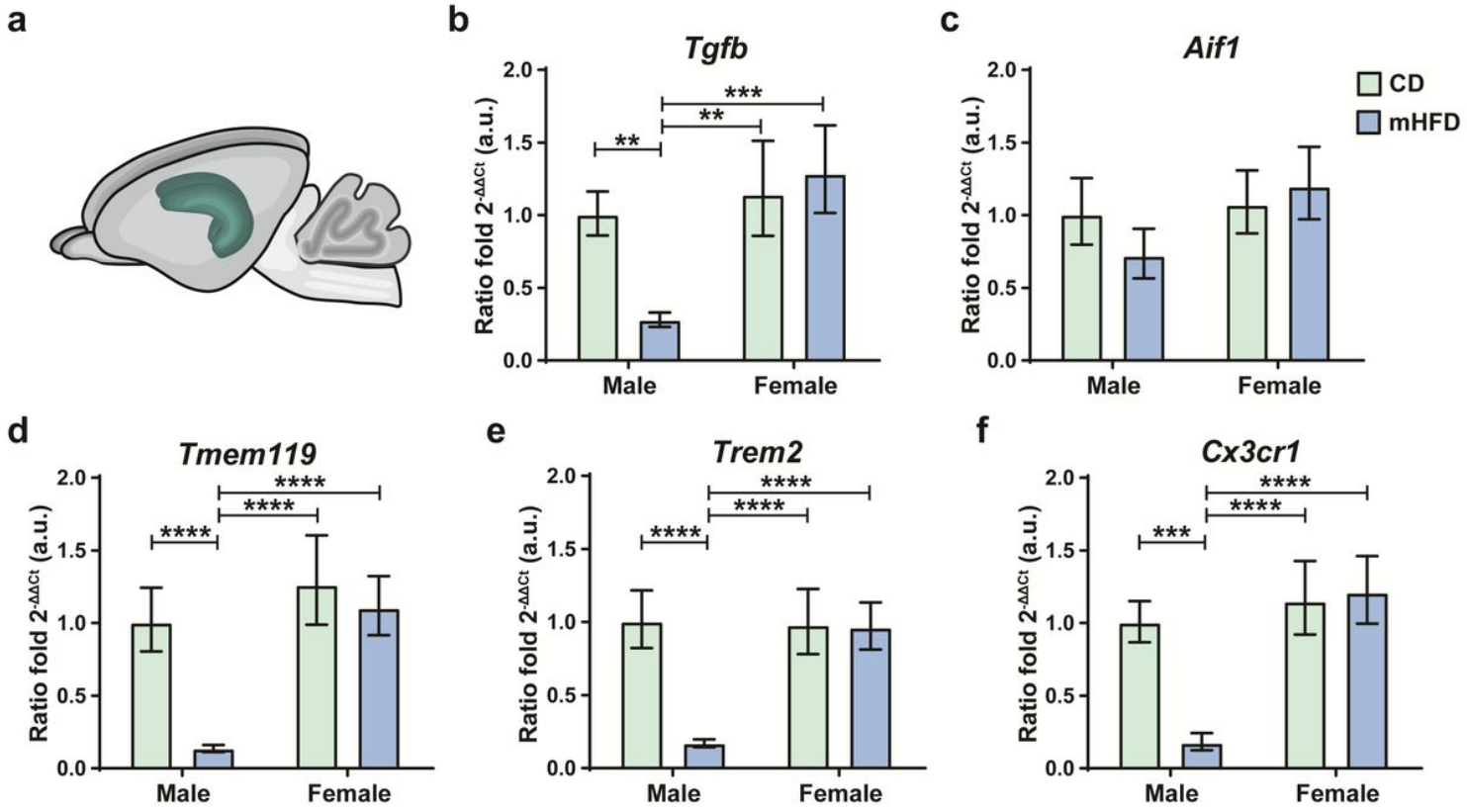

Figure 4

mHFD effect on microglia-related mRNA expression in the hippocampus of P30 offspring. (a) Scheme illustrating the region of interest, the hippocampus, in sagittal and coronal views of a mouse brain. mRNA expression (2^-ΔΔCt) was evaluated for Tgfb1 (b), Aif1 (c), Tmem119 (d), Trem2 (e) and Cx3cr1 (f) normalized by housekeeping gene Rpl32. Data are shown as 2^(-ΔΔCt Mean ± standard error of the mean). p<0.001**, p<0.001***, p<0.0001**** (sex*diet) by 2-way ANOVA followed by Bonferroni post-hoc test. Aif1: allograft inflammatory factor 1, a.u.: arbitrary units, CD: control, Ct: cycle threshold, Cx3cr1: fractalkine receptor, mHFD: maternal high-fat diet, Tgfb1: transforming growth factor β1, Tmem119: transmembrane protein 119, Trem2: triggering receptor expressed by myeloid cells 2.

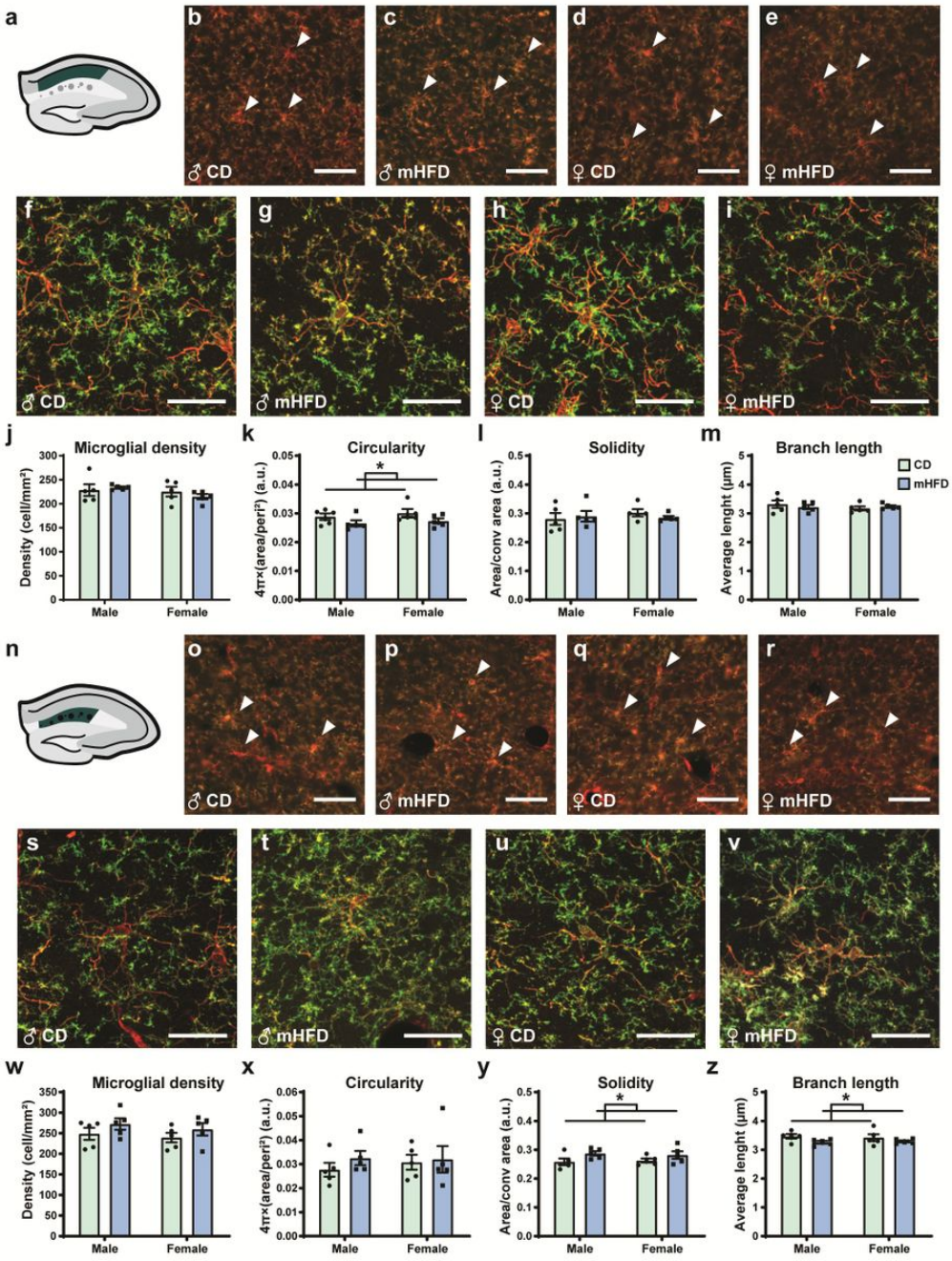

Figure 5

mHFD effect on microglial density, distribution and morphology in the dorsal hippocampus CA1 of P30 offspring. Representative scheme of the (a) st rad and (n) st lac mol to illustrate the layers analyzed. Immunofluorescence (IBA1+ low. Immunofluorescence IBA1 (red) and TMEM119 (green) allowed analysis of (b-e, o-r) microglial number and morphology (f-i, s-v). Scale bar for the density pictures is equivalent to 50µm (b-e, o-r), whereas scale bar for morphology pictures is 25µm (f-i, s-v). Only main differences are presented on the figure: (j, w) microglial density, (k,x) circularity, (l, y) solidity and (m, z) branch length average. Data are shown as mean ± standard error of the mean. P<0.05* (diet) by 2-way ANOVA. ♀: Female, ♂: male, CD: control, Conv area: convex area, mHFD: maternal high-fat diet, Peri: perimeter.

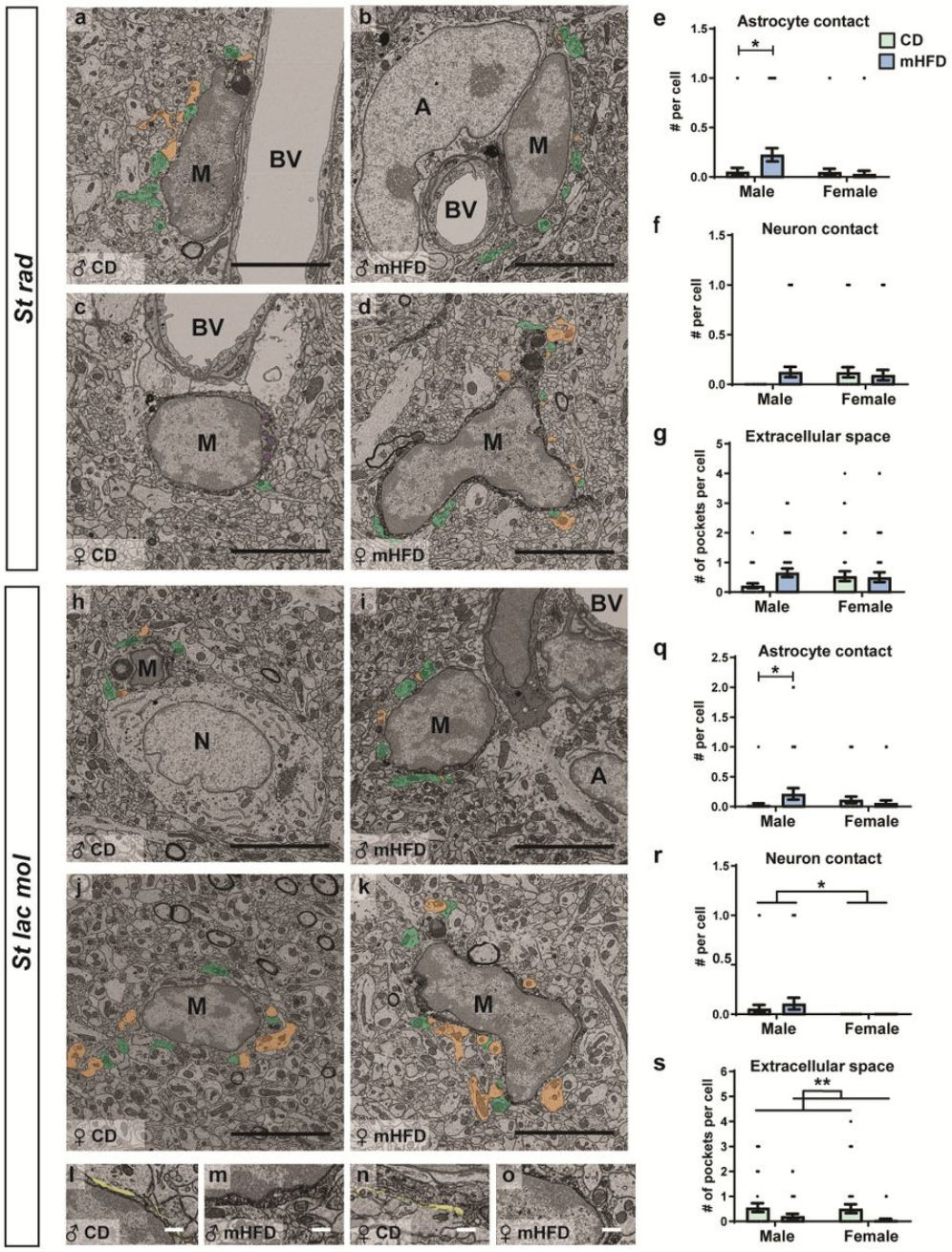

Figure 6

mHFD effect on microglial ultrastructure in the dorsal hippocampus CA1 of P30 offspring. Ultrastructural analysis of microglia was performed in the (a-g) st rad and (h-s) st lac mol. (a-d, h-k) Representative pictures of microglia as well as (l-o) higher magnification views of extracellular space pockets are provided. The interactions of microglia with their microenvironment differed between groups, here we present main results for microglial contacts with (e, q) astrocytes, (f, r) neurons and (g, s) extracellular space pockets. On the representative pictures, astrocytes, blood vessels, microglia and neurons are respectively identified by a 'A', by 'BV', by a 'M' and by a 'N'. Presynaptic and postsynaptic elements are pseudo-colored respectively in green and orange. Mitochondria are pseudo-colored in purple and extracellular space pockets in yellow. Data are shown as mean ± standard error of the mean. P<0.05* (sex) by 2-way ANOVA, p<0.05 # (sex*diet) by 2-way ANOVA followed by Bonferroni post-hoc test. ♀: Female, ♂: male, CD: control, mHFD: maternal high-fat diet.

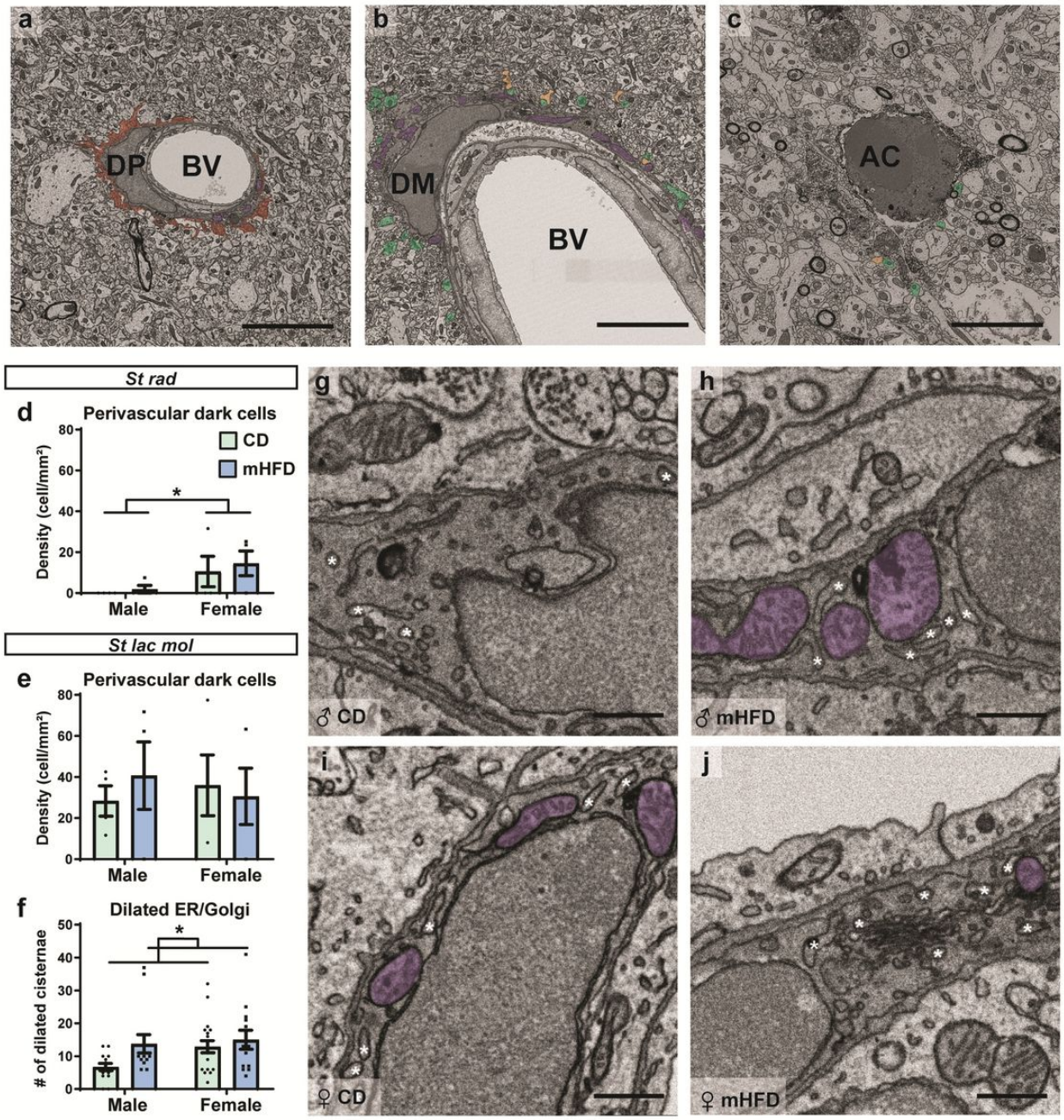

Figure 7

mHFD effect on dark perivascular cells, dark microglial cells and apoptotic cells in dorsal hippocampus CA1 of P30 offspring. (a) Dark perivascular cells, (b) dark microglia and (c) apoptotic cells examples are presented. Dark perivascular cell density was counted in the (d) st rad and the (e) st lac mol. Ultrastructural analysis of dark cells in the st lac mol revealed differences in their (f-j) dilation of the endoplasmic reticulum and Golgi apparatus cisternae. Dark processes are pseudo-colored in red. Presynaptic and postsynaptic elements are pseudo-colored respectively in green and orange. Mitochondria are pseudo-colored in purple. Blood vessel are identified by 'BV'. Dark perivascular cell, dark microglia and apoptotic cell are respectively identified using 'DP', 'DM' and 'AC'. Dilatated endoplasmic reticulum and Golgi apparatus are identified by a white asterisk. Scale bar for representative picture of cell type is equivalent to 5µm while scale bar for picture showing endoplasmic reticulum and Golgi apparatus is equivalent to 500 nm. Data are shown as mean ± standard error of the mean. $p<0.05$* (sex) by 2-way ANOVA, $p<0.05$ # (sex*diet) by 2-way ANOVA followed by Bonferroni post-hoc test. ♀: Female, ♂: male, CD: control, Dilated ER/Golgi: dilatated endoplasmic reticulum and Golgi apparatus cisternae, mHFD: maternal high-fat diet.

Supplementary Files

This is a list of supplementary files associated with this preprint. Click to download.

- SupplementaryFigure2.jpg
- SupplementaryFigure3.jpg
- SupplementaryFigure1.jpg